Materials Science and Engineering R 70 (2010) 63–91

Contents lists available at ScienceDirect

Materials Science and Engineering R

journal homepage: www.elsevier.com/locate/mser

Controlled growth and modification of vertically-aligned carbon nanotubes for multifunctional applications

Hao Chen [a], Ajit Roy [b], Jong-Beom Baek [c], Lin Zhu [d], Jia Qu [a,*], Liming Dai [d,*]

[a] Wenzhou Medical College, 270 Xueyuan Road, Wenzhou, Zhejiang 325027, China
[b] Air Force Research Laboratory, AFRL/RX, Wright-Patterson AFB, OH 45433, USA
[c] Interdisciplinary School of Green Energy and Institute of Advanced Materials and Chemicals, Ulsan National Institute of Science and Technology (UNIST), #100, Banyeon, Ulsan 689-798, Republic of Korea
[d] Department of Chemical Engineering and Department of Macromolecular Science and Engineering, Case School of Engineering, Case Western Reserve University, 10900 Euclid Avenue, Cleveland, OH 44106, USA

ARTICLE INFO

Article history:
Available online 1 July 2010

Keywords:
Carbon nanotube
Alignment
Patterning
Functionalization
Application

ABSTRACT

Vertically-aligned carbon nanotubes possess many advantages for a wide range of multifunctional applications. Along with the controlled growth of aligned/micropatterned carbon nanotubes, surface modification of vertically-aligned carbon nanotubes are essential in order to meet specific requirements demanded for particular applications. While many innovative synthetic methods have been developed for controlled growth of vertically-aligned multiwalled and single-walled carbon nanotubes, various interesting physical and chemical approaches have recently been devised for functionalization of the constituent carbon nanotubes in vertically-aligned carbon nanotube arrays with their alignment being largely retained. In this article, recent developments in the controlled growth and modification of vertically-aligned carbon nanotubes for multifunctional applications are reviewed.

Contents

* Corresponding authors.
E-mail addresses: jqu@wzmc.edu.cn (J. Qu), liming.dai@case.edu (L. Dai).

0927-796X/$ – see front matter © 2010 Elsevier B.V. All rights reserved.
doi:10.1016/j.mser.2010.06.003

1. Introduction

Carbon nanotubes (CNTs), including single- and multi-walled structures, are an attractive class of nanomaterials. While a single-walled carbon nanotube (SWNT) may be conceptually viewed as a graphene sheet that is rolled into a nanoscale tube form, a multiwalled carbon nanotube (MWNT) consists of additional graphene coaxial tubes around the SWNT core [1,2]. SWNTs show electric properties that are not shared by their multi-walled counterparts. For instance, the band gap of SWNTs can vary from zero to about 2 eV and they can exhibit metallic or semiconducting behavior, whereas MWNTs are zero-gap metals [1,2]. This is because the graphene sheet in SWNTs can be rolled up with varying degrees of twist along its length and SWNTs can have a variety of chiral structures [1–6]. Depending on their diameter and the chirality of the orientation of graphene rings along the nanotube length, SWNTs may exhibit semiconducting or metallic behavior. SWNTs also are more homogenous than their multi-walled counterparts, at least in terms of their diameters (~1 nm). Therefore, SWNTs are the promising candidate for micro-/nano-electronics. Apart from the semiconducting properties, characteristic of certain SWNTs, both SWNTs and MWNTs possess a high surface area per unit weight, good mechanical properties, high electrical conductivity at the metallic state, and high thermal conductivity/stability [1–6]. These interesting properties make CNTs very attractive for a variety of potential applications, including as conductive materials [7–11], electromagnetic and microwave absorbing coatings, high-strength composites [12–14] and fibers [15–22], sensors [23,24], field emission displays [25], energy storage and energy conversion devices [26–32], radiation sources and nanometer-sized semiconductor devices [33,34], and interconnects [33,35]. For most of the above-mentioned, and many other applications, it is highly desirable to prepare aligned/micropatterned CNTs. Particularly, vertically-aligned CNTs (VA-CNTs) can provide a well-defined large surface area, and they can be readily incorporated into device configurations. Besides, the aligned growth can produce CNT materials free-from amorphous carbons with a very narrow range of tube lengths and diameters, which is an additional advantage for some of the aforementioned, and many other, applications [1,2].

On the other hand, it has also been recognized that surface and/or interfacial properties are of paramount importance for most applications involving CNTs. However, it is very rare that CNTs with desirable bulk properties also possess the surface characteristics required for certain specific applications. Apart from the controlled growth of aligned/micropatterned CNTs, therefore, surface modification and interfacial engineering are also essential in making functional CNT materials of good bulk and surface properties as demanded for specific applications [36–42]. In this article, recent developments in the controlled growth and modification of both VA-MWNTs and VA-SWNTs are reviewed, along with discussion of their multifunctional applications.

2. Controlled growth

Carbon nanotubes synthesized by conventional techniques usually exist in a randomly entangled form [1–6]. In view of additional advantages associated with VA-CNTs for many applications, several chemical vapor deposition (CVD) methods have been developed for large-scale production of vertically-aligned single-walled, multiwalled, and super-long carbon nanotube arrays [5,6,43–46]. These VA-CNT arrays can be transferred onto various substrates of particular interest in either a patterned or non-patterned fashion. The well-aligned structure offers advantages for not only an efficient device construction but also controlled surface modification. The aligned/micropatterned growth of VA-CNTs is reviewed in this section, while the modification of VA-CNTs will be discussed in Section 3.

2.1. Vertically-aligned multiwalled carbon nanotubes (VA-MWNTs)

2.1.1. VA-MWNTs by template-synthesis

In order to construct a nanotube field emitter, de Heer et al. [47] first made an ethanol dispersion of arc-produced carbon nanotubes. These authors then passed the nanotube dispersion through an aluminum oxide micropore filter, leading to nanotubes perpendicularly aligned on the filter surface. The resultant perpendicularly-aligned nanotubes can be transferred onto the cathode substrate in a field emitting device. Similar porous membranes (*e.g.* mesoporous silica, alumina nanoholes) have also been used as a template for the so-called *template-synthesis* of VA-CNTs [48–52]. In particular, Li et al. [53] prepared the first large scale VA-MWNT array by CVD deposition of acetylene on iron nanoparticles embedded in mesoporpous silica at 700 °C (Fig. 1).

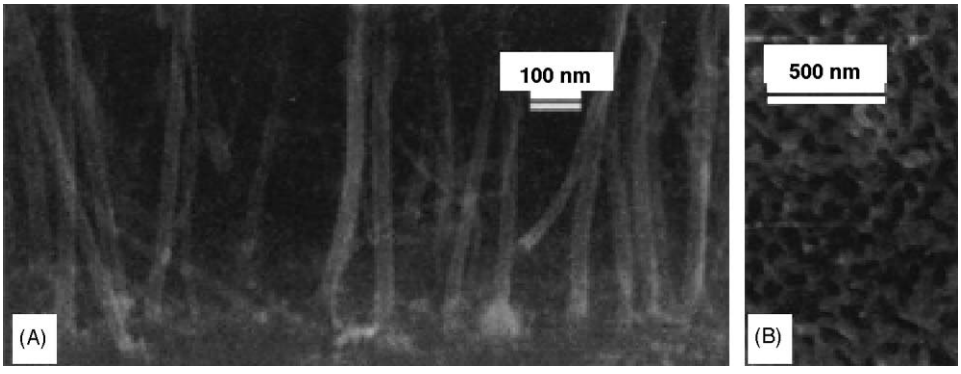

Fig. 1. (A) High-magnification scanning electron microscope (SEM) image of carbon nanotubes growing out from the mesoporous iron/silica substrate and forming an array. These carbon nanotubes have diameters of ~30 nm. Spacings between the nanotubes are ~100 nm. Most of the carbon nanotubes are aligned perpendicularly on the silica surface. (B) SEM image of the mesoporous iron/silica substrate before carbon deposition. Pores ~30 nm in diameter are distributed on the substrate and are separated by ~100 nm. Many pores have relatively regular circular openings (adapted from Ref. [53]).

The growth direction of the nanotubes could be controlled by the orientation of the pores from which nanotubes grow.

Similarly, Li and Xu [48] have also reported the controlled growth of VA-MWNTs by the pyrolysis of hydrocarbon on a nickel catalyst embedded in a porous silicon substrate. In these cases, porous silicons containing micro-, meso-, and macro-pores were produced by electrochemically etching the crystalline silicon wafer (as the anode) in an aqueous hydrofluoric acid (HF) solution (using a Pt wire as the cathode). Generally speaking, anodic aluminum oxide films can be used for producing VA-CNTs with uniform diameters and lengths by the pyrolysis of organic molecules into the well-defined nanopores either with or without a catalyst [54,55].

2.1.2. VA-MWNTs by template-free growth

Without using the template pores, many groups have reported the growth of VA-MWNTs [2]. For instance, Rao et al. [56] have prepared VA-MWNT arrays by high-temperature (*ca.* 900 °C) pyrolysis of ferrocene, which contains both metal and carbon source required for the nanotube growth. In a separate but somewhat related study, Kamalakaran et al. [57] reported the formation of VA-MWNT arrays by pyrolysis of a jet solution of ferrocene and benzene in an argon atmosphere at relatively low temperatures (*e.g.* 850 °C). As reviewed by one of the pioneers (Meyyappan et al.) [58], plasma enhanced CVD (PECVD) has been widely used to produce VA-CNTs. The PECVD even allowed the growth of individually aligned, free-standing, vertical CNTs [58]. Ren et al. [59] synthesized large arrays of VA-MWNTs by radio-frequency sputter-coating a thin nickel layer onto display glass, followed by plasma-enhanced hot filament CVD of acetylene in the presence of ammonia gas below 666 °C. Fig. 2 shows SEM images of the resultant VA-MWNT arrays. These authors have also prepared VA-MWNTs on polished polycrystalline and single crystal nickel substrates by the plasma enhanced hot filament CVD at temperatures below 666 °C [60]. The plasma density, acetylene to ammonia gas ratio, and gas flow rates were found to play important roles in regulating the diameter and uniformity of the resulting aligned CNTs. In addition to the aforementioned and some other plasma enhanced CVD techniques [61,62], microwave plasma enhanced CVD method has also been reported for synthesis of VA-MWNTs [63–65]. Unlike the plasma enhanced growth of VA-MWNTs, Avigal and Kalish et al. [66] reported a new method for the aligned growth by applying an electric field to a Co-covered substrate in a regular cold-wall chemical vapor deposition reactor (with no plasma applied) containing flowing mixture of methane and argon at 800 °C. They found that VA-MWNTs formed when a positive bias is applied to the substrate.

The formation of aligned carbon nanotubes from organic-metal complexes, containing both the metal catalyst and carbon source required for the nanotube growth, is of particular interest, as it is a one-step process involving no pre-preparation of catalyst nanoparticles on the substrate used for the nanotube growth. In this context, Dai and co-workers [67–71] have prepared large-scale aligned MWNTs perpendicular to the substrate surface by pyrolysis of iron (II) phthalocyanine, $FeC_{32}N_8H_{16}$ (designated as FePc hereafter), in an Ar/H_2 atmosphere with a dual furnace fitted with independent temperature controllers. The *as-synthesized* nanotubes align almost normal to the substrate surface and the constituent CNTs have a fairly uniform tubular length and diameter with a well-graphitized multiwall structure [69]. Depending on whether or not the catalytic particle is lifted up with the growing nanotube, two growth mechanisms, namely "tip-growth" and "base-growth", have been proposed [1,2,69]. With the FePc CVD system, we found that the growth of carbon nanotubes start from the iron catalyst particles, which consists of larger particles and smaller ones [69]. While the smaller iron particles remaining on the substrate are catalytically active to support the nanotube growth, the larger iron particles are mainly responsible for producing the carbon atomistic species from FePc vapors required for the growth of the nanotubes. The head-on contact between two adjacent large iron particles in the growth front facilitates the vertical alignment [69].

With the availability of VA-MWNTs in relatively large quantities, Zhang et al. [16,17] have recently produced CNT yarns and sheets from VA-MWNT forests in scalable quantities by continuous high-rate spinning (Fig. 3). One meter of yarn can typically be made in a few minutes. The CNT yarns and sheets are potentially useful for making transparent and highly conducting electrodes, planar sources of polarized broadband radiation, flexible organic light-emitting diodes, advanced sensors and actuators, microwave bonding of plastics, and thin film loudspeakers, to mention but a few applications [17,44,72]. CNT fibers have also been prepared by other methods [15,73–75].

2.1.3. VA-MWNTs with special architectures

As can be seen from the above discussion, a large variety of single-component VA-CNT materials have been reported for various multifunctional applications [2,5,6]. Owing to their unique one dimensional electronic structure, CNTs offer particular advantages as molecular wires for the development of nanotube nanodevices, including nanotube sensors and other optoelectronic systems. There is also a pressing need to integrate multicomponent nanoscale entities into multifunctional systems and to connect these nanosystems to the micro/macro world. Although the connection from the nanoworld to the outside world has been one of the long-standing problems in nanotechnology and still remains a big challenge, a few innovative routes to the integration

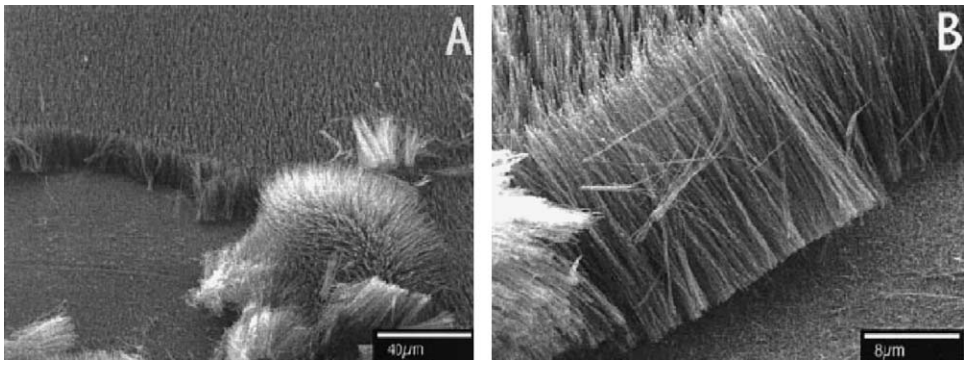

Fig. 2. (A) SEM micrograph of carbon nanotubes aligned perpendicular to the substrate over large areas. (B) Enlarged view of (A) along the peeled edge showing diameter, length, straightness, and uniformity in height, diameter, and site density (adapted from Ref. [59]).

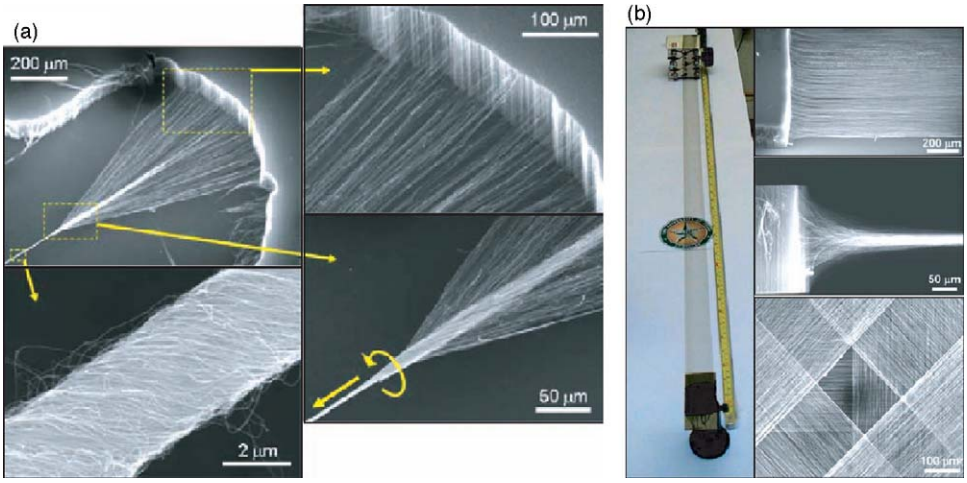

Fig. 3. SEM images showing (a) small CNT bundles simultaneously pulled and twisted from the VA-CNT forest to form CNT yarns (adapted from Ref. [16]). (b) (left) Photograph of a transparent self-supporting MWNT sheet, and (right) SEM images showing the conversion of a VA-MWNT forest into a single MWNT sheet and a two-dimensionally reinforced structure fabricated by overlaying four nanotube sheets with a 45° shift in orientation between successive sheets (adapted from Ref. [17]).

of CNTs into multidimensional and multicomponent systems have recently been devised [2].

2.1.3.1. VA-MWNT arrays with curly-entangled end-segments at the top. Along with others, Qu et al. [76] and Zhao et al. [77] have synthesized VA-CNT arrays with a straight aligning body and a curly-entangled end-segment at the top by a CVD process on a SiO_2/Si wafer. During the pyrolytic growth of the VA-MWNTs, the initially formed nanotube segments from the "base growth" process grew in random directions and form a "coiled/entangled" nanotube top layer to which the underlying straight nanotube arrays then emerged. Following earlier attempts to mimic gecko feet using microfabricated arrays of VA-CNTs [77–80], the VA-MWNT arrays produced by a low-pressure CVD process with curly-entangled end-segments at the top were demonstrated to be ideal for mimicking gecko-feet hairs [76]. In particular, Qu et al. [76] have found that the "coiled/entangled" nanotube top layer could create an anisotropic adhesion force through the sidewall contact with various substrates. It is believed that the difference between normal adhesion and shear adhesion facilitates the gecko to switch between attachment and detachment as it moves.

To demonstrate the adhesion performance of the VA-MWNTs, a small piece of the VA-MWNT film (4 mm × 4 mm, Fig. 4A), supported by a SiO_2/Si substrate used for the nanotube growth, was finger pressed from the Si side onto a vertically positioned glass slide. The nanotubes in this film have diameters ranging from 10 to 15 nm with a tube length of about 150 μm and a tube density of $\sim 10^{10}$–10^{11} cm^{-2} (Fig. 4B and C). A book of 1480 g was held onto a thin wire that was pre-glued on the back side of the SiO_2/Si substrate. An overall adhesion force of 90.7 N/cm^2 was calculated for the VA-MWNT dry adhesive film shown in Fig. 4A – which is almost ten times that of a gecko foot. Similar adhesion behaviors were observed for the VA-MWNT dry adhesive against other substrates with different flexibilities and surface characteristics, including ground glass plates, polytetrafluoroethylene (PTFE) film, rough sandpaper, and poly(ethylene terephthalate) (PET) sheet [76].

As shown in Fig. 4D, the normal adhesion force for VA-MWNT films with the tube length ranging from approximate 10–150 μm increased slightly from 10 to 20 N/cm^2. However, the corresponding shear adhesion force increased from 10 to 100 N/cm^2 over the same range of nanotube lengths. The shear adhesion force is typically several times stronger than the corresponding normal adhesion force at a constant nanotube length over about 10 μm. The high shear adhesion force of the VA-MWNT dry adhesive ensures a strong adhesion to the target surface for hanging heavy

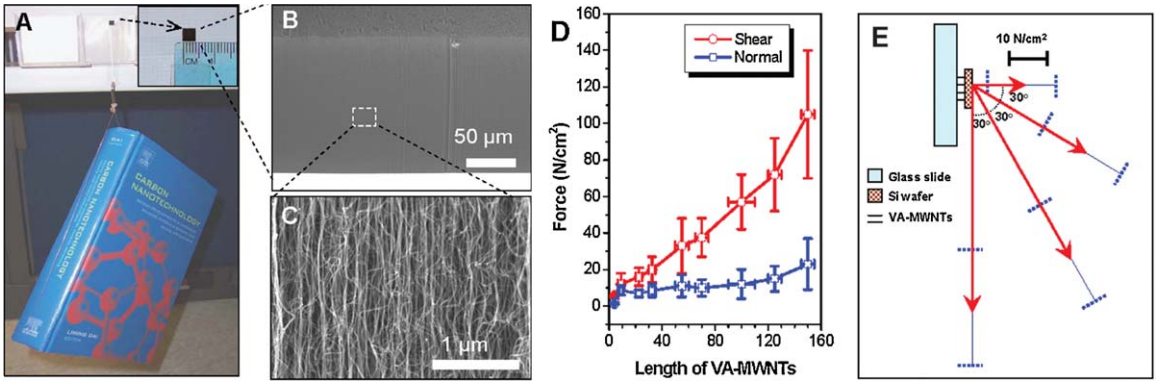

Fig. 4. (A) A book of 1480 g in weight suspended from a glass surface using VA-MWNTs supported on a silicon wafer. The top-right squared area shows the VA-MWNT array film, 4 mm × 4 mm. (B and C) SEM images of the VA-MWNT film under different magnifications. (D) Nanotube length-dependent adhesion force of VA-MWNT films attached onto the substrate with a preloading of 2 kg. The vertical and horizontal bars represent the deviations of the force and nanotube length measured for more than 20 samples of the same class, respectively. (E) Adhesion strength of VA-MWNTs with length 100 ± 10 μm at different pull-away directions. The red arrows represents the average forces measured for more than 20 samples, while the two perpendicular blue dot lines define possible deviations of the force measured for different samples of the same class. The nanotubes and substrates shown in (E) are not to scale (adapted from Ref. [76]).

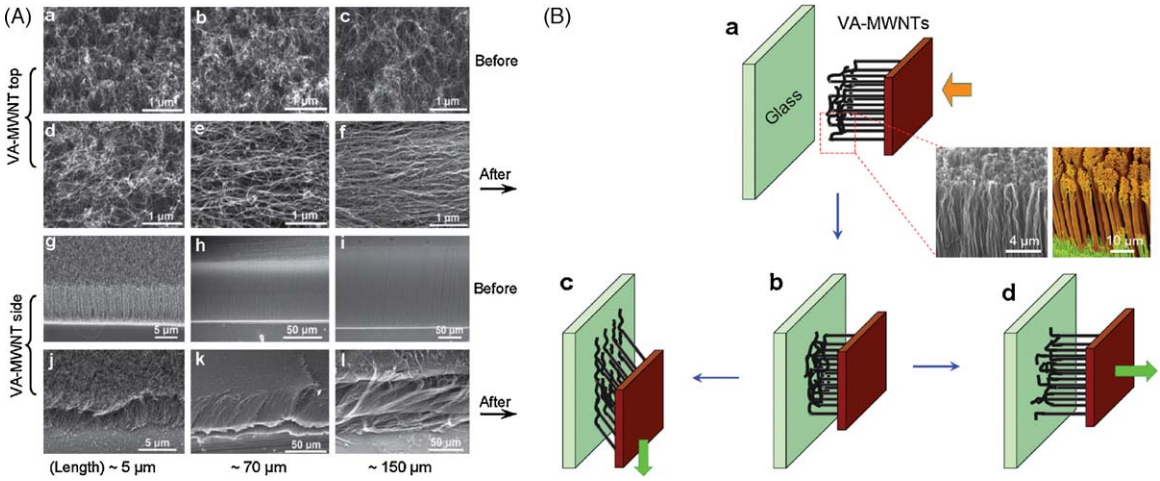

Fig. 5. (A) SEM and (B) schematic diagram for the morphological change of VA-MWNT arrays during adhesion measurements: (A) Top (a–f) and side (g–l) views of VA-MWNT films with different length before (a–c, g–i) and after (d–f, i–l) adhesion measurements. (a, d, g, j: ~5 μm; b, e, h, k: ~70 μm; c, f, i, l: ~150 μm). The arrows underneath the words of "After" indicate the shear direction during the shear adhesion force measurements. (B) Preloading (a); attachment of the VA-MWNT array onto the glass substrate (b); shear adhesion force stretching the nonaligned nanotubes on the substrate to form the "line" contact (c); normal adhesion force leading to the nonaligned nanotubes "point-by-point" peel-off from the substrate (d). Inset shows the structure similarity between the cross-section views of the VA-MWNTs and gecko's aligned elastic hairs (adapted from Ref. [76]).

objects along the shear direction, whilst a much weaker normal adhesion force allows the nanotube film to be readily detached in the normal direction. The VA-MWNT arrays were repeatedly attached and detached from the glass surface, and the supported weight did not decrease [76]. To elucidate the angular-dependence of the adhesion forces, Qu et al. [76] measured the pull-off force in various pull-away directions. The decrease in the pull-off force with increasing pull-away angle shown in Fig. 4E indicates that the shear adhesion force is much stronger than the normal adhesion force.

Qu et al. [76] further examined the morphology of the top surface and cross-sectional area of the VA-MWNT films with different tube lengths before and after the shear adhesion measurements. As expected, randomly entangled nanotube segments arising from the initial stage of the "base-growth" process were observed on the top surface of the as-synthesized VA-MWNT arrays (Fig. 5A(a–c)). After the shear adhesion force measurements, however, it was found that the top layer of the randomly entangled nanotube segments became horizontally aligned (Fig. 5A(d–f)). The degree for the shear-induced horizontal alignment increased with increasing the aligned nanotube length (Fig. 5A(d–f)). Before the testing, the nanotube "trunks" are uniformly aligned (Fig. 5A(g–i)). However, after binding on the wall, the vertically-aligned nanotube "trunks" were tilted along the shear direction (Fig. 5A(j–l)). The significant increase in the shear adhesion force with increasing aligned nanotube length observed in Fig. 4D seems to be directly related to the presence of the horizontally-aligned nanotube segments on the top surface of the VA-MWNT dry adhesive films, which formed the tube-length-dependent horizontally-aligned structure under shear.

The SEM observations are consistent with the following process. During the initial contact, the top nonaligned nanotube segments (Fig. 5B(a)) adopted randomly-distributed "line" contact with the glass substrate (Fig. 5B(b)). Upon shear adhesion force measurement (Fig. 5B(c)), the applied shear force caused the nonaligned nanotube segments to align along the shear direction on the glass substrate (Fig. 5B(c)) and the vertically-aligned nanotube "trunks" to tilt along the shear direction (Fig. 5A(j–l)), leading to a predominant aligned "line" contact with the glass surface (Fig. 5A(d–f)). During the normal adhesion force measurements, however, the top nonaligned nanotube segments contacted with the glass substrate were peeled from the substrate through a "point-by-point" detaching process (Fig. 5B(d)), requiring a much lower force than that for pulling off the entire nanotube array (Fig. 4D). This anisotropic force distribution ensures strong binding along the shear direction and easy lifting in the normal direction. This finding should open many technological applications, ranging from new types of athletic shoes and car tires that have an unusual grip, to creating window-clinging suits like Spider-Man's, to sealing packages to bonding electronic and even aerospace vehicle parts in outer space where traditional polymer-based adhesives would be dried up and failed under the vacuum environment.

2.1.3.2. VA-MWNT arrays with Y-shaped at the top. Using branched nanochannel alumina templates, Li et al. [81] have produced Y-shaped carbon nanotubes by the pyrolysis of methane over cobalt-covered magnesium oxide (Fig. 6). In this case, these authors first prepared the template with Y-branched nanochannels by anodizing a highly pure aluminum sheet in 0.3 M oxalic acid at 10 °C under a constant voltage of 50 V for 15 h, which resulted in an hexagonal array of pores near the aluminum surface. After chemically removing the original film, a second anodization was performed under the same conditions, typically for 30 min. The anodization voltage was then reduced to about 35 V. Because the pore cell diameter is proportional to the anodization voltage, reducing the voltage by a factor of 1/2 resulted in twice as many pores appearing in order to maintain the original total area of the template, and nearly all the pores branched into two, smaller-diameter pores. As a consequence, the resulting template consisted of parallel Y-branched pores with stems about 90 nm in diameter and branches about 50 nm in diameter. Y-shaped CNTs have potential applications in electronic and micro-/nano-fluidic devices (*e.g.* electron interferometry) [82,83].

2.1.3.3. VA-MWNT arrays with ZnO nanoparticles at the top. 1D heterojunction structures based on nanomaterials are of significance to both fundamental nanoscience [2,84] and potential applications in nanoscale systems, including various new electronic and photonic nanodevices [85–88]. Consequently, considerable effort has been made in recent years to devise and characterize various heterojunctions between different low-dimensional nanomaterials [89–91]. Examples include the syntheses of multiwalled CNT–zinc sulfide heterojunctions by a combination of ultrasonic and heat treatments [92], CNT–silicon

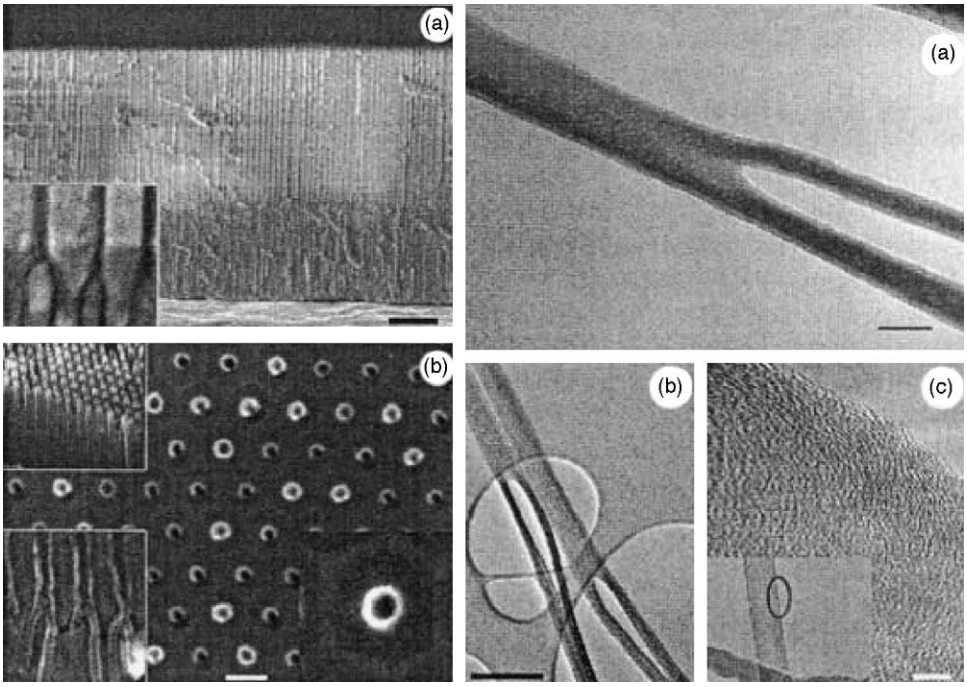

Fig. 6. Left: (a) SEM image of a Y-branched nanochannel template (scale bar: 1 μm). The inset shows where the Y branches start to grow. (b) Top-view SEM image of carbon nanotubes aligned in the template after ion-milling of amorphous carbon on the surface (scale bar, 100 nm). The nanotube diameter is larger than the original pore owing to thermal expansion of the template during growth. Top inset, stem part of the Y-junction tubes. Bottom left inset, close-up of the region between stem and branch portions still embedded in the template. Bottom right inset, close-up of the top of the nanotube in its hexagonal cell. Right: transmission electron microscope (TEM) image of (a) the Y-junction tube (scale bar, 50 nm) with a stem of about 90 nm and branches 50 nm in diameter. (b) Y-junction formed by using higher anodization voltages, resulting in stems of about 100 nm and branches 60 nm in diameter (scale bar: 200 nm). (c) High-resolution TEM image of a typical Y-junction nanotube wall showing graphitic multiwall structure (scale bar, 5 nm). Inset shows the part of the tube that was imaged (adapted from Ref. [81]).

nanowire heterojunctions by localizing a suitable metal catalyst at the end of a preformed nanotube or nanowire [85], and SWNT–gold nanorod heterojunctions through the selective solution growth of Au nanorods on an SWNT structure [93]. Among them, CNT-based 1D heterojunctions are of particular interest because of the unique molecular geometry as well as excellent electronic, thermal, and mechanical properties intrinsically associated with CNTs [2,4,94]. However, the growth of VA-CNT heterojunction arrays was a big challenge. Liu et al. [95] have reported the synthesis of large-scale vertically aligned CNT–ZnO heterojunctions simply by water-assisted chemical vapor deposition of carbon on a zinc foil, which acts as both the substrate for the VA-CNT growth and zinc source for the formation of the ZnO nanostructures. Water, as a weak oxidizer, provides the oxygen

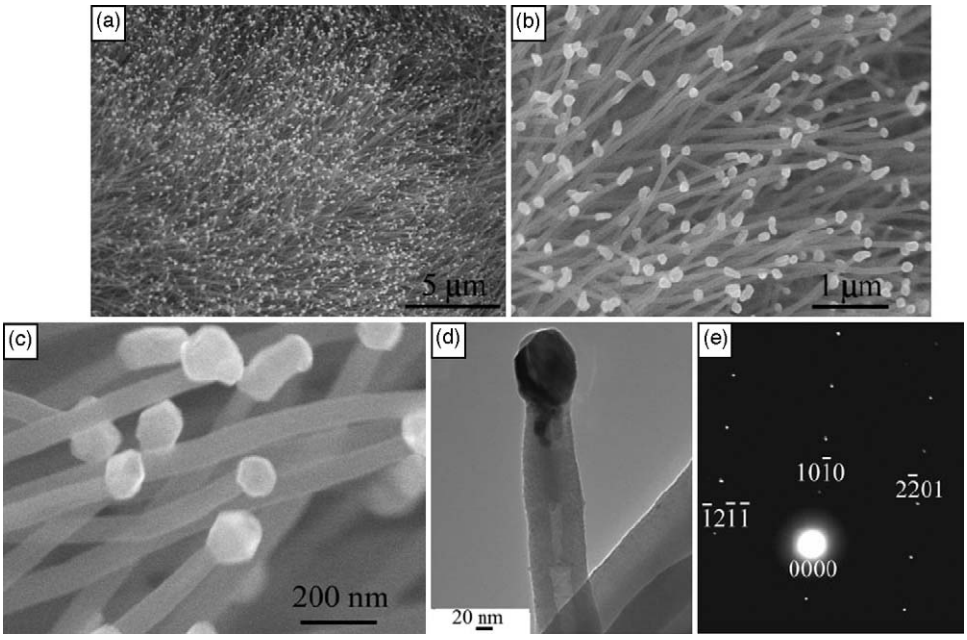

Fig. 7. (a) Low-magnification SEM image of a vertically aligned CNT–ZnO heterojunction array. (b and c) As for (a), under higher magnification. (d) TEM image of a typical CNT–ZnO heterojunction and (e) a selected-area electron diffraction (SAED) pattern of a ZnO tip (adapted from Ref. [95]).

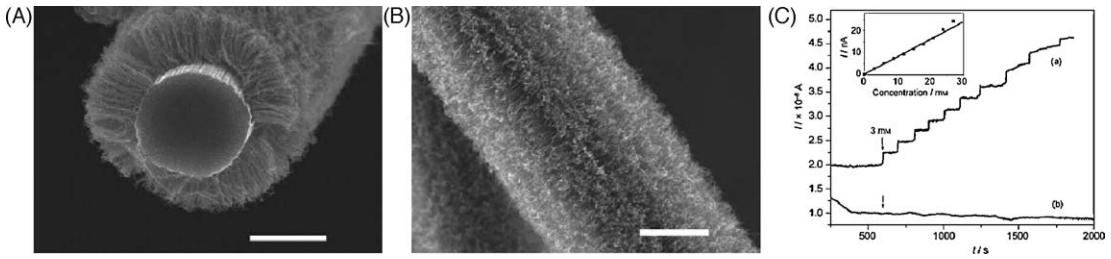

Fig. 8. Cross-sectional (A) and side-view (B) SEM images of the CNT-CFs. Scale bars for (A and B): 5 μm. (C) Amperometric responses to successive additions of 3 mM glucose for (a) the glucose-oxidase-attached aligned CNT–CF electrode, and (b) the CF electrode after having been subjected to the same electrochemical oxidation and glucose oxidase immobilization processes. The inset shows a plot for current increment against glucose concentration for the CNT–CF glucose sensor (adapted from Ref. [98]).

source for the formation of ZnO nanostructures and also enhances CNT growth [43].

Fig. 7a shows a low-magnification SEM image of the as-synthesized CNT–ZnO sample, revealing a large-scale vertically-aligned array. Although the corresponding SEM images under higher magnification in Fig. 7b and c show some misalignment at the top of the nanotube array, Fig. 7b clearly shows the CNT–ZnO heterojunction with a ZnO crystal (bright spot) attached on the tip of each of the constituent VA-CNTs. Fig. 7c further reveals that approximately 40% of the ZnO nanoparticles are of hexagonal morphology. The corresponding TEM image in Fig. 7d shows that the CNT thus prepared is multiwalled, and that the ZnO nanoparticle is intimately connected to the aligned CNT structure. Fig. 7e shows the selected-area electron diffraction (SAED) pattern of the ZnO nanoparticle, which indicates that the *as-prepared* ZnO nanoparticle is single crystalline and can be indexed as hexagonal wurtzite ZnO [96]. The intimately connected heterojunctions between the aligned CNTs and ZnO nanostructures thus prepared possess interesting optoelectronic properties attractive for many potential applications [95], including their use as field emitters and electro-optic sensors and detectors.

2.1.3.4. Carbon fibers sheathed with VA-MWNT arrays. The growth of VA-CNTs around carbon-fibers provides a new class of multidimensional and multicomponent nanomaterials with well-defined surface and interfacial structures attractive for a wide range of potential applications. Thostenson et al. [97] were the first to modify the surface of pitch-based carbon fiber by growing CNTs directly on carbon fibers. More recently, Qu et al. [98] have developed an effective approach for the preparation of multidimensional hybrid structures with individual microsized carbon fibers (CFs) sheathed by VA-MWNTs generated via pyrolysis of FePc, and demonstrated their potential applications in various electrochemical systems. Fig. 8A and B shows SEM images for CFs with a diameter of 7 μm surrounded by FePc-generated VA-MWNTs in either a patterned or nonpatterned fashion. For these hybrid CF-CNT coaxial structures, the carbon microfiber can be used as a microelectrode to connect the surrounding VA-CNTs to the outside world. Consequently, the resultant microsized CFs sheathed with VA-CNTs could offer a useful platform for the development of multidimensional and multifunctional nanomaterials and devices of practical significance. To demonstrate the potential of the CNT-sheathed CFs for biosensing, Qu et al. [98] have attached glucose oxidase molecules onto electrochemically-induced carboxylic groups on the CF-supported CNTs via classical carbodiimide chemistry. The glucose oxidase-grafted VA-CNTs on the CF were then used to detect glucose in a 0.1 M phosphate buffer solution (pH 7.4) at room temperature by electrochemically probing hydrogen peroxide generated from glucose oxidation with glucose oxidase. Amperometric responses for the glucose oxidase-immobilized VA-CNTs on the CF substrate and the pristine CF electrode to each successive addition of 3 mM glucose are shown in Fig. 8C. While there is no obvious current change with the addition of glucose for the CF electrode (curve (b) of Fig. 8C), a stepwise increase in the current signal upon each successive addition of glucose was observed for its VA-CNT coated counterpart (curve (a) of Fig. 8C). The inset in Fig. 8C shows the current increment with the glucose concentration for the CNT–CF electrode, which shows a pseudo-linear relationship indicating a high sensitivity and reliability. The electrochemical detection of glucose using the glucose oxidase-containing CNT electrode involves oxidation of hydrogen peroxide from glucose oxidation [98]. Given that many enzymatic reactions are associated with the generation of hydrogen peroxide, the above

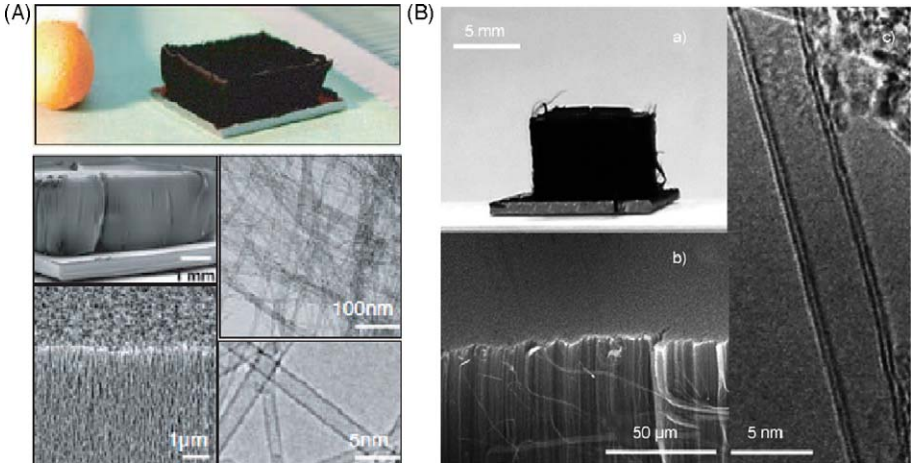

Fig. 9. (A) SEM and TEM images of SLVA-SWNT forests prepared by the water-assist growth method (adapted from Ref. [43]). (B) (a) A digital photograph, (b) SEM image, and (c) TEM image of the super-long double-walled CNTs (adapted from Ref. [46]).

methodology should be applicable to sense many other biologically important substances.

2.1.4. Superlong vertically-aligned carbon nanotubes (SLVA-CNTs)

Recent advances in CVD techniques have facilitated the growth of super-long vertically aligned carbon nanotubes (SLVA-CNTs) with millimiter-order lengths (up to 10 mm). Despite some controversies in the role of H_2O molecules [99,101] in the water-assisted CVD reported by Hata et al. [43], several groups have reproduced vertically-aligned super-long multiwalled (double-walled) and even single-walled CNTs, as exemplified in Fig. 9 [43,46,101–103].

SLVA-CNTs offer significant advantages over their shorter counterparts for various potential applications, including multifunctional composites, sensors, and nanoelectronics [46]. In addition, their millimeter-order lengths provide novel opportunities for translating electronic, thermal, and other physical properties through individual nanotubes over large length scales.

2.2. Vertically-aligned single-walled carbon nanotubes (VA-SWNTs)

2.2.1. VA-SWNTs by template-free growth

As can be seen from the above discussion, the growth of VA-MWNTs has been studied for some years. However, it is only the recent effort to grow VA-SWNTs [43,45,104,105]. The slow progress in the VA-SWNT growth is largely caused by the difficulty in preparing densely packed small catalyst particles (~1 nm in diameter) that do not aggregate into bigger ones at the high temperature required for the aligned growth of SWNTs [43,45,78,99–110]. Amama et al. [100] demonstrated that the addition of H_2O into the nanotube-growth CVD system prevented Fe catalyst particles from aggregation through Ostwald ripening due to retarded diffusion rates of the catalyst atoms by the water-induced surface oxygen and hydroxyl species. After the seminal work reported by Hata et al. [43,104], several groups have recently reported the growth of VA-SWNTs [45,99–110]. In particular, Qu and Dai [45] have exploited the growth of VA-SWNTs by combining PE-CVD with fast heating. This method facilitated the growth of SWNTs in the form of large scale aligned arrays without the need for any additional H_2O or O_2. In a typical experiment, a thin film of Fe (1 nm) was sputter-deposited onto a SiO_2/Si wafer pre-coated with a 10-nm-thick Al layer. The Al coating was used to effectively prevent the Fe catalyst from aggregation for supporting the PE-CVD growth of VA-SWNTs by quickly moving (<5 s) the catalyst-coated SiO_2/Si wafer into the center of a plasma-enhanced tube furnace under a mixture gas of H_2/CH_4. Fig. 10a shows a typical SEM image of VA-SWNT arrays produced by the combined PE-CVD and fast heating method. As can be seen in Fig. 10a, the as-synthesized nanotubes aligned almost normal to the substrate surface and have a fairly uniform tubular length. The corresponding cross-sectional view under a higher magnification shows that the *as-grown* nanotubes were very clean and formed into loosely-packed "bundles" (Fig. 10b). A Raman spectrum of the as-synthesized sample recorded with a 785 nm laser (Fig. 10c) clearly shows the strong resonant radial breathing modes (RBM) of SWNTs in the range of 130–280 cm^{-1}. The clear separation of the G peaks at *ca.* 1570 and 1600 cm^{-1} seen in Fig. 10c is also a characteristic for SWNTs [99]. The high value of ~12 for the G-band to D-band intensity ratio suggests a high degree of graphitization for the as-synthesized VA-SWNT arrays. Qu and Dai [45] have also performed Raman measurements on the as-synthesized SWNT sample using the 514 nm laser (Fig. 10c), which can probe both semiconducting and metallic SWNTs and is often used to estimate their relative contents [111–115]. The much stronger RBM peaks in the range of *ca.* 150–210 cm^{-1}, attributable to semiconducting nanotubes, than those over *ca.* 210–280 cm^{-1}, characteristic of metallic nanotubes, indicate that the as-synthesized SWNT sample contains a high percentage of the semiconducting nanotubes. In view of the fact that SWNTs (either semiconducting or metallic) of different diameters resonate with laser beams of different excitation wavelengths [2], multiple excitation wavelengths, including the 633 nm laser [116], have been used for the Raman measurements on the as-synthesized SWNT sample [117]. A TEM image of individual nanotubes dispersed from an ethanol solution also reveals that the nanotubes thus prepared are SWNTs mostly free from amorphous carbon (Fig. 10d).

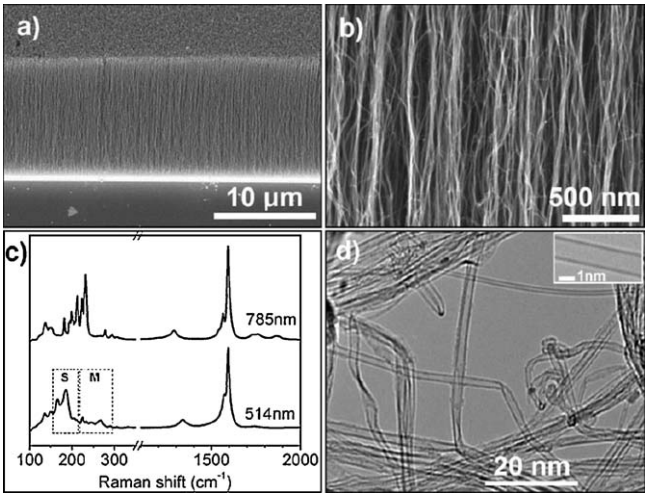

Fig. 10. SEM images (a, b), Raman spectra (c), and TEM image (d) of VA-SWNTs synthesized on a SiO_2/Si wafer pre-coated with a 1-nm Fe/10-nm Al under a 80 W/13.56 MHz plasma and 0.14 H_2/CH_4 partial pressure ratio at 750 °C for 20 min. The dashed rectangles in (c) define the approximate regions for metallic (M) and semiconducting (S) Raman features of SWNTs. Inset of (d) shows a higher magnification TEM image of an individual nanotube (adapted from Ref. [45]).

2.2.2. Preferential growth of semiconducting VA-SWNTs

One of the major hurdles for the widespread application of SWNTs in semiconductor electronics is the coexistence of metallic and semiconducting carbon nanotubes in the as-synthesized samples. Due to the presence of metallic nanotubes, field effect transistor (FET) characteristics (*e.g.* the on/off ratio and integration uniformity) become poor and uncontrollable. Therefore, it will be a significant advancement if *semiconducting* VA-SWNT arrays suitable for electronic applications (*e.g.* FETs) can be directly synthesized. Indeed, certain CVD methods with and without the plasma enhancement have been used to preferentially produce nonaligned SWNTs with a high percentage of semiconducting nanotubes (~90%) [118,119] or SWNTs with a specific chirality distribution [120–125]. Due to the random feature of nonaligned SWNTs, however, it is difficult to further increase the percentage of semiconducting nanotubes necessary for the high-throughput construction of electronic devices. Although the mechanism for preferentially growing the semiconducting SWNTs is still not well understood, these pioneering studies indicate the possibility for selective syntheses of semiconducting SWNTs by carefully controlling the growth parameters. In this context, Qu et al. [117] have developed a modified PE-CVD and fast heating method for the preferential growth of *semiconducting* VA-SWNTs using a low pressure (30 mTorr) C_2H_2 flow as carbon source without additional carry gas. From Raman measurements using laser beams of multi-wavelengths, about 96% of semiconducting nanotubes in the as-grown VA-SWNT array was estimated. The as-synthesized semiconducting VA-SWNTs can be directly used as the electronically active material in FET devices, even without any purification or separation.

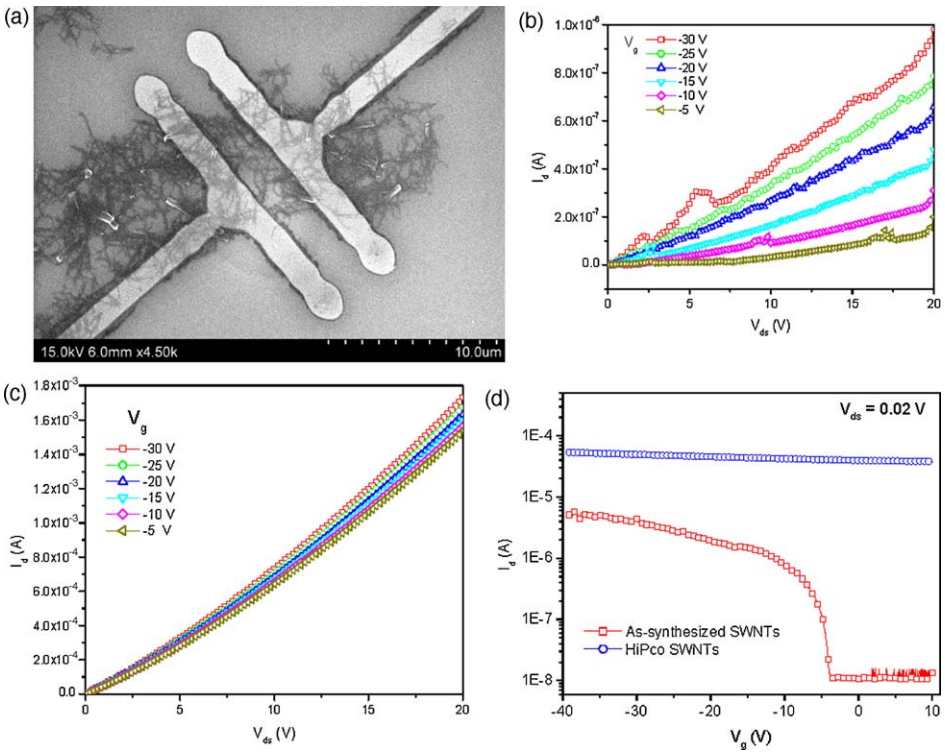

Fig. 11. (a) A typical SEM image of the preferentially synthesized SWNT bundle network on two electrodes; Drain current *vs* drain voltage measured at gate voltages ranging from −30 to −5 V in 5 V steps for (b) the as-synthesized SWNT FET and (c) HiPco network device; and (d) drain current *vs* gate voltage for both the as-synthesized SWNT (□) and HiPco (○) network devices measured at a drain voltage of 0.02 V (adapted from Ref. [117]).

To construct the nanotube FETs, Qu et al. [117] dispersed 0.1 mg of the as-synthesized VA-SWNTs in 1 mL DMF under ultrasonication for 10 min, followed by solution-casting the slightly dispersed nanotube bundles between the drain and source Au electrodes prefabricated on a SiO_2/Si wafer (400-nm-thick SiO_2) to form a nanotube bundle network FET with the Si substrate as a bottom gate electrode (Fig. 11a). For comparison, these authors have also prepared a network FET based on HiPco SWNTs according to the same procedure. They deliberately chose bundled nanotubes instead of individual nanotubes for the FET investigation in order to demonstrate the high percentage of semiconducting nanotubes in the as-grown VA-SWNT sample.

As can be seen in Fig. 11b, FETs based on SWNTs grown by the preferential synthesis showed a typical field effect characteristic with the drain current increasing with increasing negative gate voltage, indicating a p-type semiconductor for the SWNTs. In contrast, Fig. 11c shows almost no field effect for the corresponding HiPco device. The variations of drain current with the gate voltage for a drain voltage of 0.02 V given in Fig. 11d show an on/off ratio of more than 100 for the as-synthesized SWNT FET in air and a quasi-linear plot with a relatively small slope for the HiPco device. The on/off ratio of more than 100 for the as-synthesized SWNT network FET is comparable to that of planar FETs consisting of parallel SWNTs after electrical breakdown of metallic nanotubes [126].

Due also to the similar length-scale between the nanotube length and channel width, the presence of any metallic nanotubes in the semiconducting SWNT matrix could cause a short-circuit problem for the FET. However, it did not happen in this case. Therefore, these results clearly indicate the high yield of semiconducting nanotubes in the as-synthesized VA-SWNT sample. The mobility (μ) of the as-synthesized SWNTs was estimated, according to the standard formula [127–130], to be *ca.* 11.4 $cm^2\ V^{-1}\ s^{-1}$ in air, which is slightly higher than that of a planar FET after electrical breakdown of metallic nanotube [131,132]. These preferentially-grown *semiconducting* VA-SWNT arrays should be attractive for the development of various optoelectronic nanodevices with high performance.

2.3. VA-MWNT micropatterns

2.3.1. VA-MWNT micropatterns by photolithography

The preparation of micropatterned VA-CNTs is of paramount importance to many potential applications related to nanotube devices, ranging from new electron field emitters in panel displays [47], to nanotube sensor chips [132], to molecular filtration membranes [51]. Along with many reported approaches for fabricating micropatterns of *randomly-oriented* carbon nanotubes [133–136], the preparation of carbon nanotube patterns with constituent nanotubes *aligned normal* to the substrate surface has also been discussed [5,6,25,67,68] - albeit to a less extent. For example, Fan et al. [25] reported the first synthesis of regular arrays of oriented nanotubes on Fe-patterned porous silicon by pyrolysis of ethylene (Fig. 12). These well-ordered nanotubes were demonstrated to be useful as electron field emitters.

On the other hand, Yang et al. [68] developed a micropatterning method for photolithographic generation of the VA-MWNT arrays with resolutions down to a micrometer scale. Fig. 13 shows the steps of the photolithographic process (Fig. 13A), along with a typical SEM image of the resultant VA-MWNT micropattern (Fig. 13B).

These authors first photolithographically patterned a positive photoresist film of diazonaphthoquinone (DNQ)-modified cresol novolak (Fig. 13C(a)) onto a quartz substrate. Upon UV irradiation through a photomask, the DNQ-novolak photoresist film in the exposed regions was rendered soluble in an aqueous solution of sodium hydroxide due to photogeneration of the hydrophilic indenecarboxylic acid groups from the hydrophobic DNQ via a photochemical Wolff rearrangement [137] (Fig. 13C(b)). They then carried out the pyrolysis of FePc, leading to region-specific growth of the aligned carbon nanotubes in the UV exposed regions (Fig. 13B). In this case, the photolithographically patterned

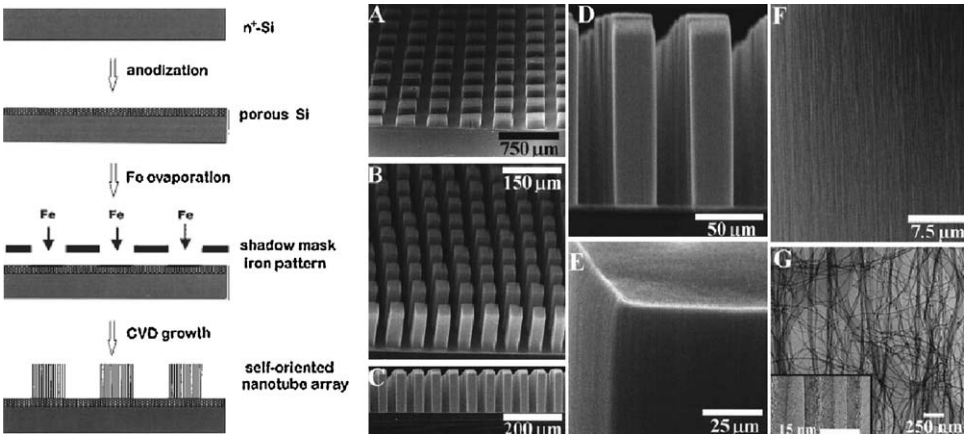

Fig. 12. (Left panel) Schematic process for the synthesis of regular arrays of vertically-aligned nanotubes on porous silicon by catalyst patterning and CVD. (Right panel) Electron micrographs of self-oriented nanotubes synthesized on n-type porous silicon substrates. (A) SEM image of nanotube blocks synthesized on 250 μm × 250 μm catalyst patterns. The nanotubes are 80 μm long and oriented perpendicular to the substrate [see (F)]. (B) SEM image of nanotube towers synthesized on 38 μm by 38 μm catalyst patterns. The nanotubes are 130 μm long. (C) Side view of the nanotube towers in (B). The nanotubes self-assemble such that the edges of the towers are perfectly perpendicular to the substrate. (D) Nanotube "twin towers", a zoom-in view of (C). (E) SEM image showing sharp edges and corners at the top of a nanotube tower. (F) SEM image showing that nanotubes in a block are well aligned to the direction perpendicular to the substrate surface. (G) TEM image of pure multiwalled nanotubes in several nanotube blocks grown on a n-type porous silicon substrate. Even after ultrasonication for 15 min in 1,2-dichloroethane, the aligned and bundled configuration of the nanotubes is still evident. The inset is a high-resolution TEM image that shows two nanotubes bundling together. The well-ordered graphitic lattice fringes of both nanotubes are resolved (adapted from Ref. [25]).

photoresist film, after an appropriate carbonization process, acted as a shadow mask for the patterned growth of the aligned nanotubes as the polymer micropattern did not allow for the Fe nanoparticle deposition due probably to a surface tension mismatch. This method is fully compatible with existing photolithographic processes [138].

2.3.2. VA-MWNT micropatterns by soft-lithography

Soft-lithography has become a very promising technique for micro-/nano-structuring a wide range of materials [139–141]. Various strategies, including microcontact printing (μCP), mechanical scraping, and micromolding, have been developed for nanoscale patterning that otherwise is difficult by photolithography [142]. Using a poly(dimethylsiloxane) (PDMS) elastomer stamp, μCP has been shown to be a convenient method for generating self-assembled monolayer (SAM) patterns of certain "molecular inks" (*e.g.* alkanethiol, alkylsiloxane) on appropriate substrate surfaces (*e.g.* gold, silver, copper, aluminum, and silicon dioxide) [143–145]. Alternatively, the solvent-assisted micromolding (SAMIM) technique allows pattern formation through

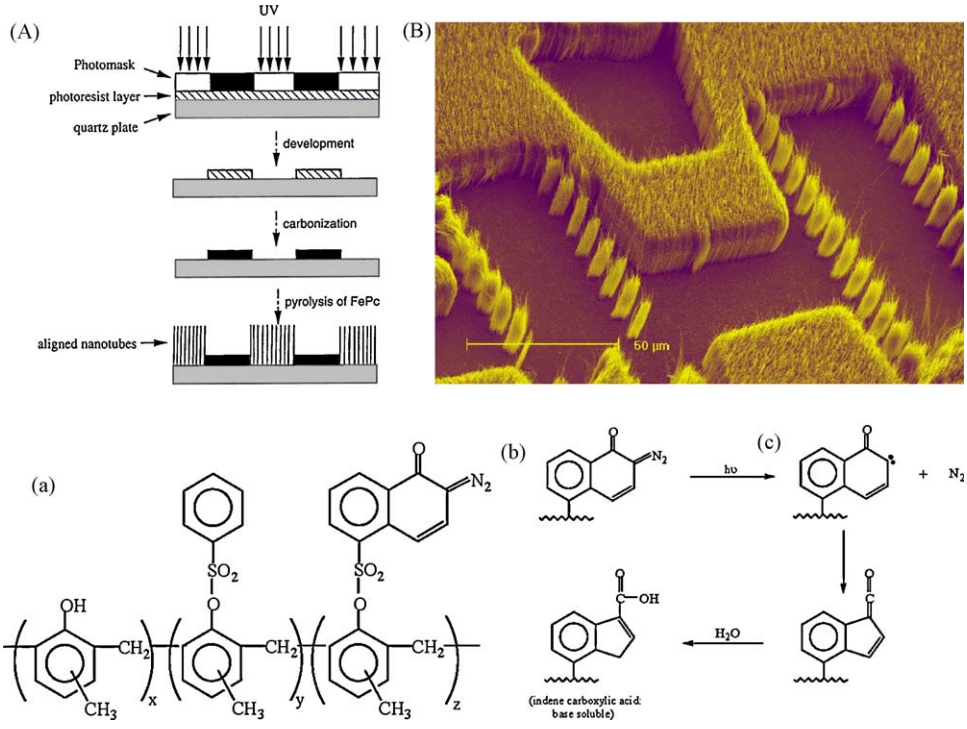

Fig. 13. (A) Schematic representation of the micropattern formation of VA-MWNTs by photolithographic process. (B) Typical SEM micrographs of patterned films of VA-MWNTs prepared by the pyrolysis of FePc onto a photolithographically prepatterned quartz substrate. (C) (a) Molecular structure of the DNQ-Novolak photoresist, and (b) photochemical reactions of the DNQ-Novolak phoresist (adapted from Ref. [68]).

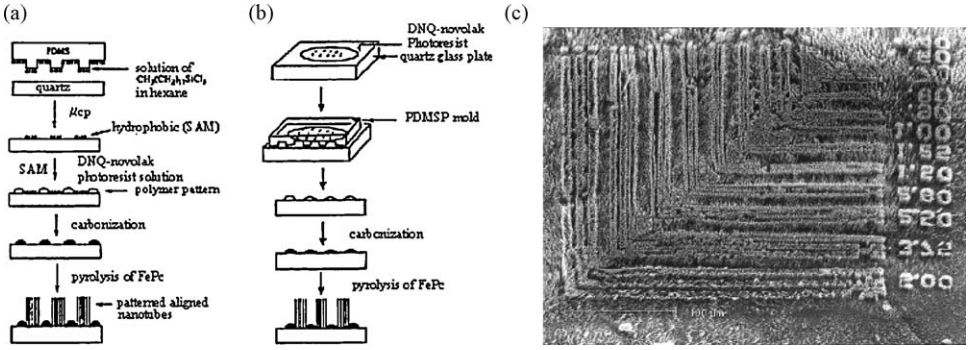

Fig. 14. Schematic illustration of the procedure for fabricating patterns of VA-MWNTs by (a) microcontact printing, (b) solvent assisted micromolding, and (c) a typical SEM image of a VA-MWNT micropattern prepared by the pyrolysis of FePc onto the quartz substrate prepatterned with photoresist by micromolding technique (Scale bar: 100 μm, adapted from Ref. [70]).

solvent evaporation from a thin layer of polymer solution confined between a PDMS elastomer mold and a substrate surface [146,147].

In addition to the photolithographic patterning described above, Huang et al. [70] used the micro-contact printing (μCP) and micro-molding techniques to prepare micropatterns of carbon nanotubes aligned in a direction normal to the substrate surface. While the μCP process involves the region-specific transfer of self-assembling monolayers (SAMs) of alkylsiloxane onto a quartz substrate and subsequent adsorption of polymer chains in the SAM-free regions (Fig. 14a), the micro-molding method [148] allows the formation of polymer patterns through solvent evaporation from a precoated thin layer of polymer-solution confined between a quartz plate and a PDMS elastomer mold (Fig. 14b). The DNQ-Novolak photoresist patterns formed by both the microcontact printing and solvent assisted micromolding were then carbonized into carbon black for region-specific growth of the aligned nanotubes in the polymer-free regions (Fig. 14c) by pyrolysis of FePc under Ar/H_2 atmosphere at 800–1100 °C, as is the case for the above mentioned photolithographic patterning [68]. The spatial resolution is limited by the resolution of the mask used. Micropatterns of aligned nanotubes prepared by soft-lithography have resolutions down to 0.8 μm [70], suitable for fabrication of various electronic and photonic devices. The ease with which micro-/nano-patterns of organic materials can be made on curved surfaces by the soft-lithographic techniques [140,141] should provide additional benefits to this approach with respect to the photolithographic method, especially for the construction of flexible devices, as demonstrated in more recent studies [149–154].

2.3.3. VA-MWNT micropatterns by plasma patterning

As demonstrated above, the photolithographically or soft-lithographically patterned polymer film, after an appropriate carbonization process, can act as a shadow mask for the region-specific growth of VA-CNT micropatterns as the carbonized film cannot support the nanotube growth while the polymer-free quartz surface allows for the growth of VA-MWNTs by pyrolysis of FePc [68,70]. However, both the photolithographic and soft-lithographic patterning methods involve a tedious carbonization process prior to the aligned nanotube growth. In order to eliminate the carbonization process, Chen and Dai [71] have prepared carbon nanotube arrays aligned in a direction normal to the substrate surface by radio-frequency glow-discharge plasma (RFGD) polymerization of a thin polymer pattern onto a quartz substrate (Fig. 15A), followed by region-specific growth of the VA-MWNTs in the plasma-polymer-free regions by pyrolysis of FePc (Fig. 15B).

The highly-crosslinked structure of plasma-polymer film [155,156] should ensure the integrity of the plasma polymer layer, even without carbonization, at high temperatures necessary for the nanotube growth from FePc [71] to allow the pristine plasma-polymer micropattern to act as a shadow mask for the patterned growth of the aligned nanotubes, as is the case with the photolithographic and soft-lithographic patterning [68,70]. Therefore, the carbonization process involved in the previous work on photolithographic [68] and soft-lithographic [70] patterning of the aligned carbon nanotubes can be completely eliminated in the plasma patterning process. Owing to the generic nature of the plasma polymerization, many other organic vapors can also be used efficiently to generate plasma polymer patterns for the patterned growth of the aligned carbon nanotubes.

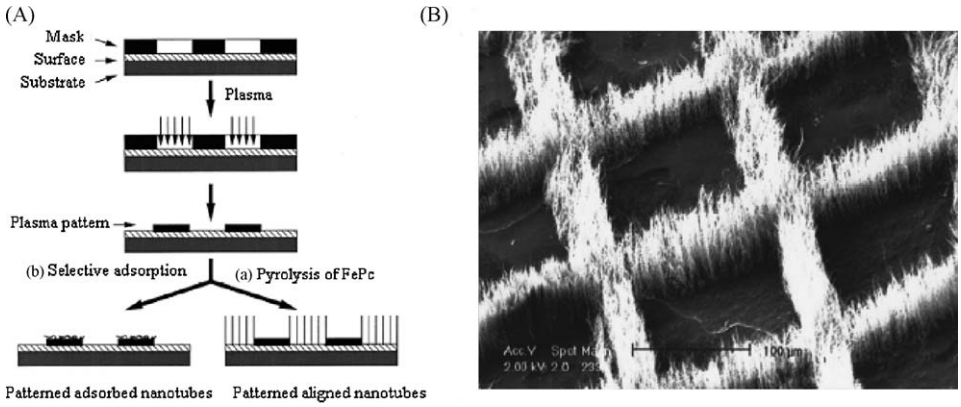

Fig. 15. (A) Schematic illustration of the procedure for fabricating patterns of carbon nanotubes by (a) plasma polymerization followed by aligned nanotube growth, and (b) plasma activation followed by region-specific adsorption of nanotubes. (B) SEM images VA-MWNT arrays growing out from the plasma-polymer-free regions on an *n*-hexane-plasma-polymer-patterned quartz plate (adapted from Ref. [71]).

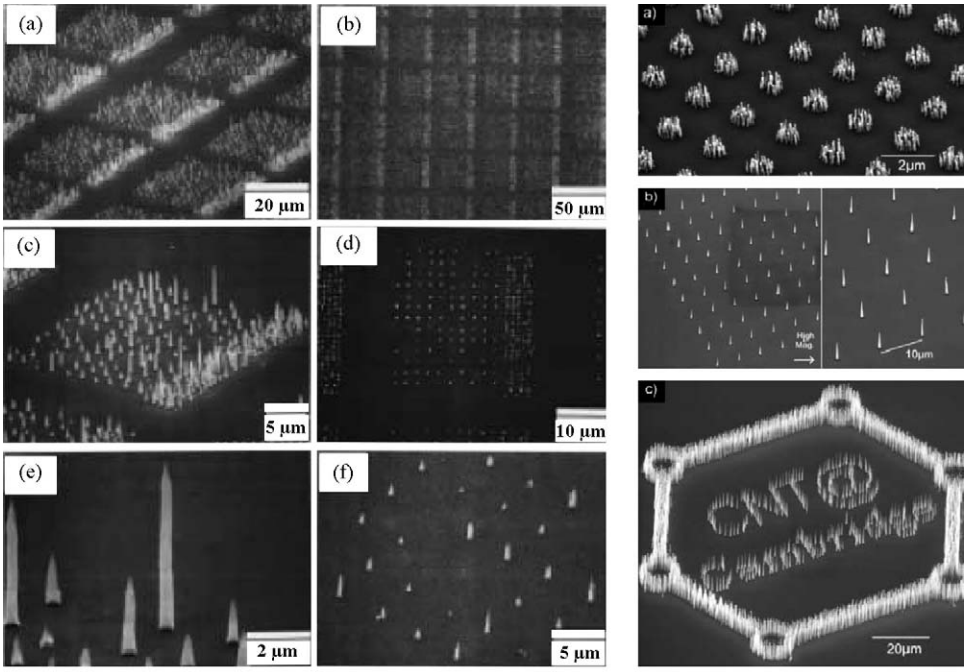

Fig. 16. (A) A series of SEM images from different viewing angles showing the growth of carbon nanotube obelisks on an array of submicron nickel dots. (a) An inclined view of a repeated array pattern. (b) A top (normal) view of a repeated array pattern. (c) An inclined view of one array pattern. (d) A top (normal) view of one array pattern. (e) A magnified view along the edge of one pattern. (f) An inclined view of carbon obelisks grown on nickel dots separated by 5 μm (adapted from Ref. [157]). (B) (a) Bunches of aligned carbon nanotubes (about 100 nm) are deposited on 1 μm nickel dots by breaking up the nickel catalyst film into multiple nanoparticles. (b) Single aligned nanotubes are deposited when the nickel dot size is reduced to 100 nm as only a single nickel nanoparticle is formed from the dot. (c) The selective growth of high yield and uniform aligned nanotubes with different densities (adapted from Ref. [159]).

2.3.4. VA-MWNT micropatterns by e-beam lithography

Along with the aforementioned soft-lithography, e-beam lithography has also been exploited to produce VA-CNT micropatterns with a nanoscale resolution. For instance, Ren and co-workers [157,158] reported the growth of freestanding VA-MWNTs onto a grid of patterned submicron nickel dot(s) by plasma-enhanced hot-filament CVD using acetylene gas as the carbon source and ammonia as the dilution gas. Individual VA-MWNTs were observed to grow well on the grid (Fig. 16A). A thin film nickel grid was fabricated on a silicon wafer by electron beam lithography and metal evaporation. Using this method, freestanding VA-MWNTs suitable for certain specific applications, such as scanning microscopy probes and electron emitters, were fabricated [157,158]. Teo et al. [159] also fabricated a uniform array of single, free-standing VA-MWNTs by PE-CVD on substrate patterned with nickel catalysts by either photolithography or electron-beam lithography (Fig. 16B) [159].

Electron-beam deposited catalysts have also been used to produce aligned carbon nanotubes with other controlled structures [160–162]. Besides, Sohn et al. [163] have also used a similar method to produce aligned carbon nanotubes on Fe nanoparticles deposited by a pulsed laser on a porous Si substrate. These authors found that the growth characteristics of the carbon nanotubes depended strongly on the Fe film deposition (by the pulse-laser) time [163].

2.3.5. VA-MWNT micropatterns with 3D architectures

Using a modified photolithographic method for patterned pyrolysis of FePc, Chen et al. [164] have prepared three-dimensional (3D) micropatterns of VA-MWNTs on the substrate surface with region-specific tubular lengths and packing densities. The photoresist system used in this approach consists of novolac/hexamethoxymethyl melamine (HMMM) as the film former, phenothiazine (RH) as the photosensitizer, and diphenyliodonium hexafluorophosphate ($Ph_2I^+X^-$) as a photoacid generator that can photochemically generate the acid, through a photomask, required for the region-specific crosslinking of the photoresist film [165]. Fig. 17A represents the steps of the photolithographic process with the associated photochemical reactions.

UV irradiation through a photo-mask creates a latent acid pattern formed by the photolithographic generation of acid from $Ph_2I^+X^-$ (Reaction 1 of Fig. 17B). Post-exposure baking at 110 °C for 10 min caused an acid-induced crosslinking of the novolac resin and HMMM (Reactions 2 and 3 of Fig. 17B), rendering the photoresist film in the UV-exposed regions insoluble in an aqueous solution of sodium hydroxide (3 wt%) and ethanol (10 wt%). In contrast, the photoresist film in the regions unexposed to the UV light was removed simply by immersing in the developer solution for 10–20 s, leading to the formation of a negative polymer pattern on the substrate. The crosslinking reactions between HMMM and novolac resin were further completed by immersing the photoresist patterned substrate into an aqueous solution of *p*-toluenesulfonic acid (10 wt%) for 30 min and further baked at 150 °C for 30 min [165]. The photoresist pre-patterned silica wafer or quartz plate was then directly used as the substrate for region-specific growing of VA-MWNTs without carbonization.

Fig. 17C represents a typical SEM image of the 3D VA-MWNT micropatterns thus prepared, which clearly shows a region-specific packing density and tubular length. Owing to the highly crosslinked structure between the novolac resin and HMMM within the photoresist patterns, the integrity of the photoresist layer was maintained, even without the carbonization, at the high temperatures required for the aligned nanotube growth from FePc [67]. In contrast to the DNQ-novolak photoresist film, the resultant HMMM-crosslinked novolac photoresist film supported the nanotube growth due, most probably, to its delicate surface characteristics that allowed the Fe nanoparticles to deposit onto this particular photoresist layer at the initial stage of the FePc

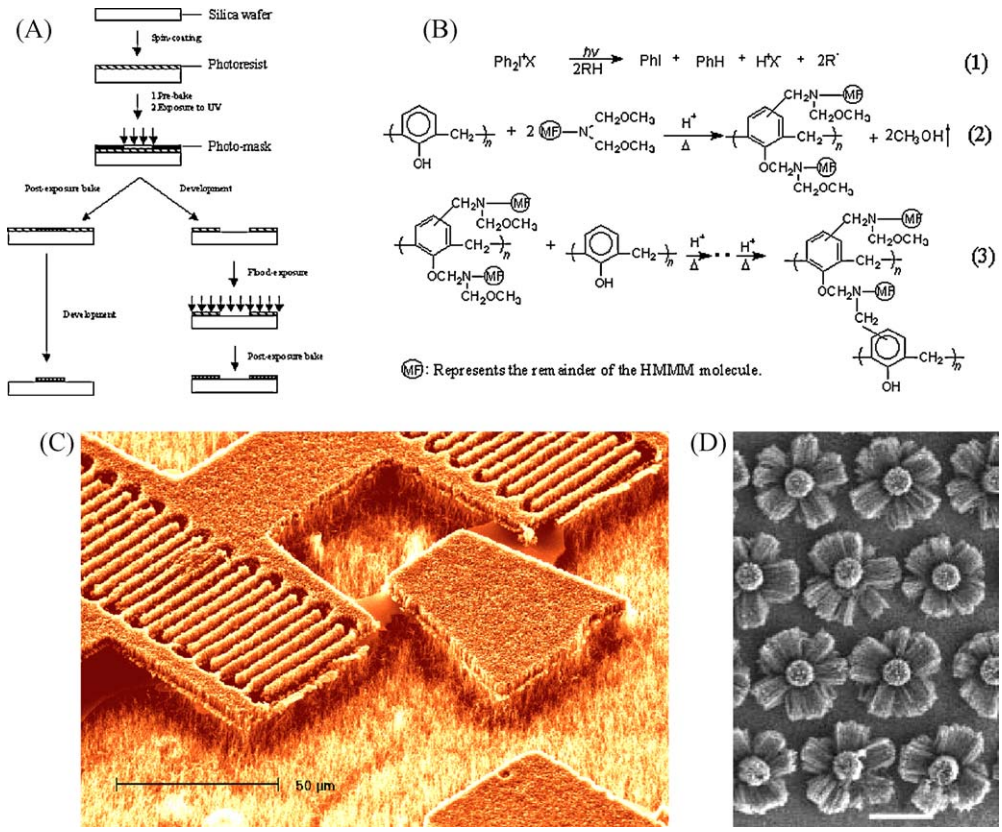

Fig. 17. (A) Schematic illustration of the procedures for photolithographic pattering the chemically amplified photoresist into a negative and positive pattern. (B) photochemical reactions of the novolac/HMMM photoresistor. (C) A typical SEM micrograph of the 3D aligned carbon nanotube micropattern (adapted from Ref. [164]). (D) Multidimensional aligned carbon nanotubes grown out from SiO_2 polygons prepatterned on a Si substrate (Scale bar: 50 μm, adapted from Ref. [167]).

pyrolysis [67]. Different surface characteristics between the photo-exposed and non-exposed areas led to different nanotube growth rates, and hence the 3D growth. The 3D micropatterns of aligned carbon nanotubes thus prepared offer the possibility for construction of advanced microdevices with multidimensional features.

On the other hand, Ajayan and co-workers [166,167] have reported the highly substrate dependent site-selective growth of VA-MWNTs by CVD on patterned SiO_2/Si substrates using conventional lithography. SEM results indicated that CNTs grew on the SiO_2 substrate, with no observable growth on the Si substrate. On this basis, these authors have used photolithography to pattern a silicon surface with silica (SiO_2) polygons to allow the VA-MWNTs to grow out in several different directions at once (Fig. 17D).

2.4. Multicomponent VA-CNT micropatterns

With the recent developments in nanoscience and nanotechnology, there is a pressing need to integrate multicomponent nanoscale entities into multifunctional materials and devices. In this regard, Yang et al. [168] have reported a dry contact transfer technique for preparing multicomponent carbon nanotube micropatterns, in which COOH-containing non-aligned MWNTs were region-selectively adsorbed within the heptylamine-plasma-treated areas interposed into the patterned structure of VA-MWNTs [71,169]. More recently, these authors have also demonstrated the formation of multicomponent carbon nanotube micropatterns with self-assembled nonaligned MWNTs interdispersed within the patterned structure of VA-SWNTs [170]. The integration of

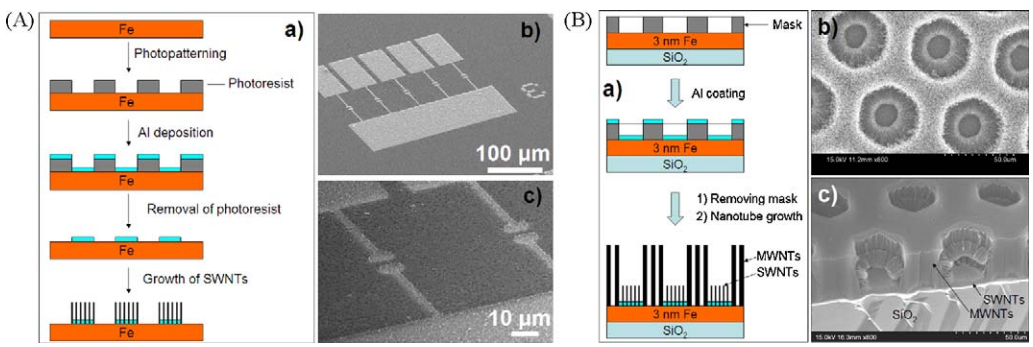

Fig. 18. (A) (a) Schematic representation of photopatterning Al on a commercially-available iron foil for the growth of VA-SWNTs, and (b, c) SEM imgaes of the VA-SWNT micropatterns at different magnifications. (B) (a) Schematic representation of Al patterning on a Fe-coated substrate for the patterned growth of three-dimensional, interposed VA-SWNTs and VA-MWNTs. (b, c) Top and side view of the 3D VA-MWNT/VA-SWNT micropatterns (adapted from Ref. [45]).

additional nanocomponent(s) into VA-CNT micropatterns thus demonstrated could lead to novel multicomponent/multifunctional materials and devices described below and in Section 3, though the microfabrication of multicomponent VA-CNT micropatterns is still a research field in its infancy.

2.4.1. Multicomponent VA-CNT micropatterns by direct growth

Recently, Qu and Dai [45] have found that VA-SWNTs can be synthesized on Al-activated bulk iron foil while VA-MWNTs grew well on the Al-free iron substrate by PE-CVD of C_2H_2 at 750 °C. Consequently, they proceeded to grow VA-SWNT micropatterns by region-selective coating a thin layer of Al on the bulk iron substrate. As shown in Fig. 18A(a), they used a photopatterning method to region-selectively depositing Al on a commercially-available bulk iron foil, after electropolishing, for patterned growth of VA-SWNTs. Fig. 18A(b and c) show SEM images recorded at different magnifications for the VA-SWNT arrays thus prepared. As can be seen, VA-SWNT micropatterns having a close replication of the photomask structure with aligned nanotubes growing only in the Al covered regions, suitable for microelectronic device fabrication, are clearly evident.

Apart from the growth of VA-SWNTs on iron foils by the Al activation described above, Qu and Dai [45] also found that thin Fe catalyst coating (3–5 nm) on conventional substrates (*e.g.* SiO_2/Si wafer) used for the growth of VA-MWNTs can also be activated to grow VA-SWNTs by pre-coating with a thin layer of Al. This finding, together with Al patterning, enabled them to readily prepare multicomponent micropatterns with the Al-activated VA-SWNTs interposed within the patterned VA-MWNT arrays on an Fe pre-coated substrate (*e.g.* SiO_2/Si wafer). Fig. 18B(a) shows the steps for patterned deposition of an Al thin coating through a TEM grid (as the physical mask) onto a SiO_2/Si wafer pre-coated with a 3-nm thick Fe film to support the region-selective growth of VA-SWNTs over the Al covered areas and VA-MWNTs in the Al-free regions. Fig. 18B(b) shows a top view of the resultant nanotube micropattern, in which the hexagonal windows of the TEM grid "mask" were replicated, while the side view in Fig. 18B(c) clearly shows the shorter VA-SWNTs interposed within the hexagonal areas surrounded by longer VA-MWNTs. The observed length difference between the region-selectively-grown VA-SWNTs and VA-MWNTs resulted mainly from their different growth rates and catalyst lifetimes. The single-walled and multiwalled nanotube characteristics of those shorter VA-SWNTs and longer VA-MWNTs within the 3D multicomponet nanotube micropatterns shown in Fig. 18B(b and c) were confirmed by area-selected micro-Raman spectra (spot size ≈2 μm). The newly-prepared multicomponent

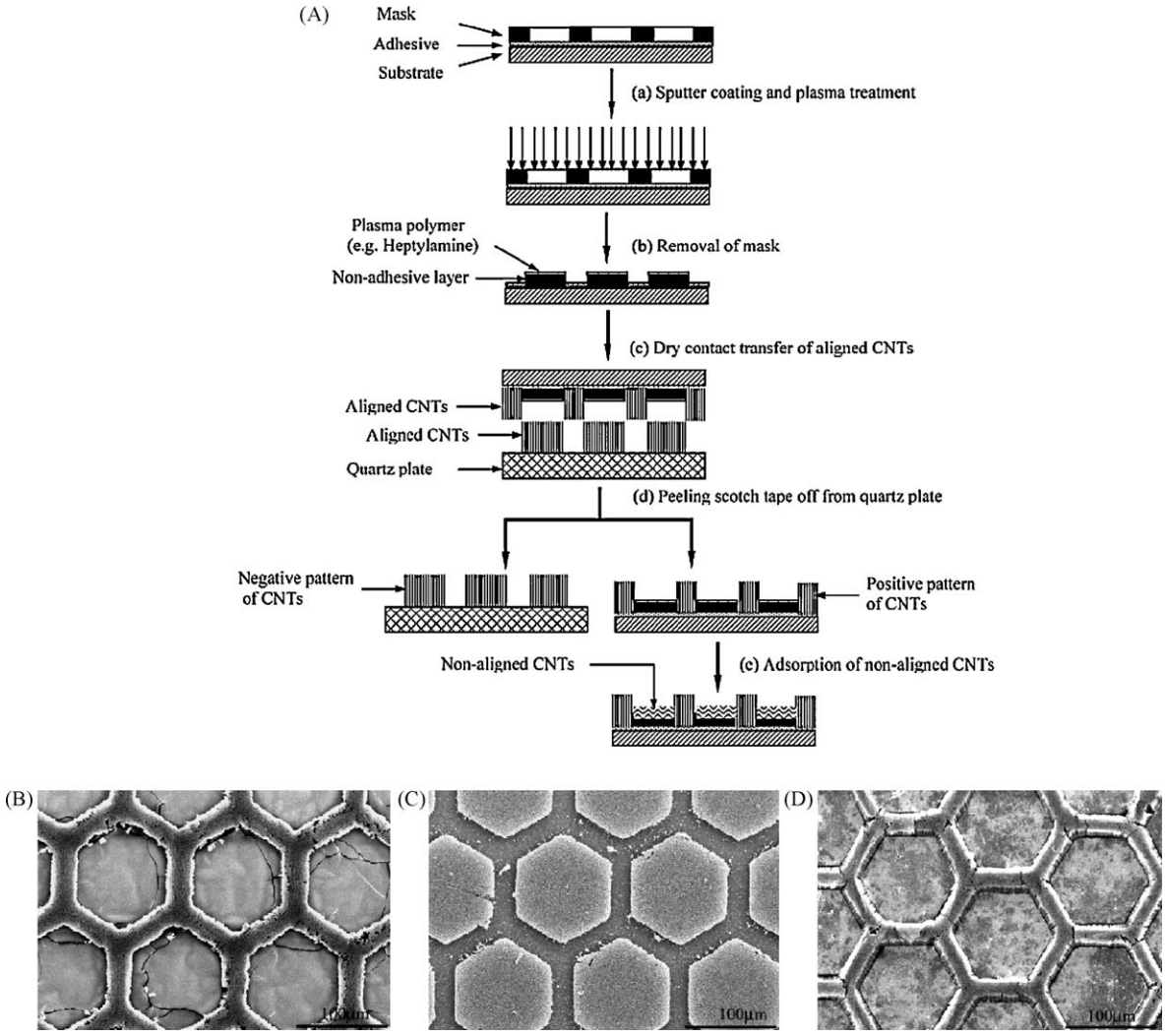

Fig. 19. (A) Schematic illustration of the procedures for fabricating multicomponent interposed carbon nanotube micropatterns by dry contact transfer, followed by region-specific adsorption. SEM images of (B) VA-CNT patterns after being transferred onto the Scotch tape (*i.e.* positive pattern), (C) VA-CNT patterns left on the quartz plate after the dry contact transfer (*i.e.* negative pattern), and (D) the multicomponent interposed carbon nanotube micropatterns with the nonaligned carbon nanotubes region-specifically adsorbed between VA-CNT patterns within hexagonal regions (adapted from Ref. [168]).

3D VA-MWNT/VA-SWNT interposed micropatterns could serve as useful building blocks for fabricating multifunctional micro-/nano-electronics with region-specific features while the conducting substrate provides a direct electrical contact.

2.4.2. Multicomponent VA-CNT micropatterns by contact transfer

Micropatterns of VA-CNTs have also been prepared by simply pressing an adhesively sticky tape (*e.g.* Scotch tape) prepatterned with a nonadhesive layer onto a nonpatterned aligned nanotube film, followed by peeling off the sticky tape from the quartz substrate in a dry state [168]. Fig. 19A shows the steps used for micropatterning the Scotch tape with a thin layer of silver, the subsequent plasma treatment of the silver surface, the contact transfer of the aligned carbon nanotubes, and the region-specific adsorption of nonaligned carbon nanotubes. As expected, the nanotubes underneath the silver-free regions were selectively transferred onto the Scotch tape as a positive image of the TEM grid used as a physical mask (Fig. 19B) whereas those covered by the silver-patterned areas remained on the quartz substrate as a negative pattern (Fig. 19C). As can be seen in Fig. 19B and C, the integrity of those carbon nanotubes (*e.g.* alignment, packing density) transferred onto the Scotch tape is almost the same as the as-grown nanotubes remaining on the quartz plate. However, the newly transferred carbon nanotubes with a robust aligned and/or micropatterned structure are supported by a flexible substrate. The crack edges seen within the hexagonal areas in Fig. 19B were, most probably, caused by mechanical deformation of the silver layer when the overlaying flexible Scotch tape was pressed downward to the nanotube film during the transfer process. Although some care may be needed to prepare the aligned carbon nanotube micropatterns with interposed crack-free silver patterns on flexible Scotch tape, the soft nature of the Scotch tape used for the dry contact transfer should allow for the development of multicomponent nanotube micropatterns for flexible device applications.

In conjunction with the region-specific surface modification, this dry contact transfer method has further led to the production of multicomponent carbon nanotube micropatterns in which different components are interposed in an intimate fashion [168,170]. This was exemplified by the resultant micropatterns with self-assembled nonaligned carbon nanotubes interdispersed into the discrete areas in the patterned structure of VA-CNTs (Fig. 19D). Using different sputter-coating layers and chemistries for the region-specific adsorption, multicomponent micropatterns of VA-MWNTs interposed with nanoparticles or other nanomaterials have also been produced [168,170]. The above demonstration of the formation of multicomponent interposed VA-CNT micropatterns by the contact-transfer micropatterning technique could thus be very attractive for applications of carbon nanotubes in various micro- to nano-meter scale optoelectronic devices and many other systems.

3. Controlled modification

3.1. Modification of VA-CNTs by plasma and photochemical activation

As can be seen from the above discussion, VA-CNTs (either in patterned or nonpatterned forms) are promising as new multifunctional materials for a variety of potential applications. However, it is very rare that VA-CNTs with desirable bulk properties also possess the surface characteristics required for specific applications. Along with nanoaligned CNTs, therefore, research on VA-CNTs has also been extended to include chemical modification. For nonaligned CNTs, the tips of CNTs have been shown to be more reactive than their sidewalls. The treatment of CNTs with certain acids (*e.g.* refluxing in HNO_3 [171–174] and/or H_2SO_4 [175–177] was demonstrated to open the nanotube tips and to introduce –COOH and –OH groups at the opened ends [178–180]. Besides, various covalent chemistries have been developed to functionalize the CNT sidewalls. Examples include the covalent fluorination of CNTs within the temperature range between 250 and 400 °C [181–186] or derivatization of them with certain highly reactive chemicals such as dichlorocarbene [187,188]. Due to the

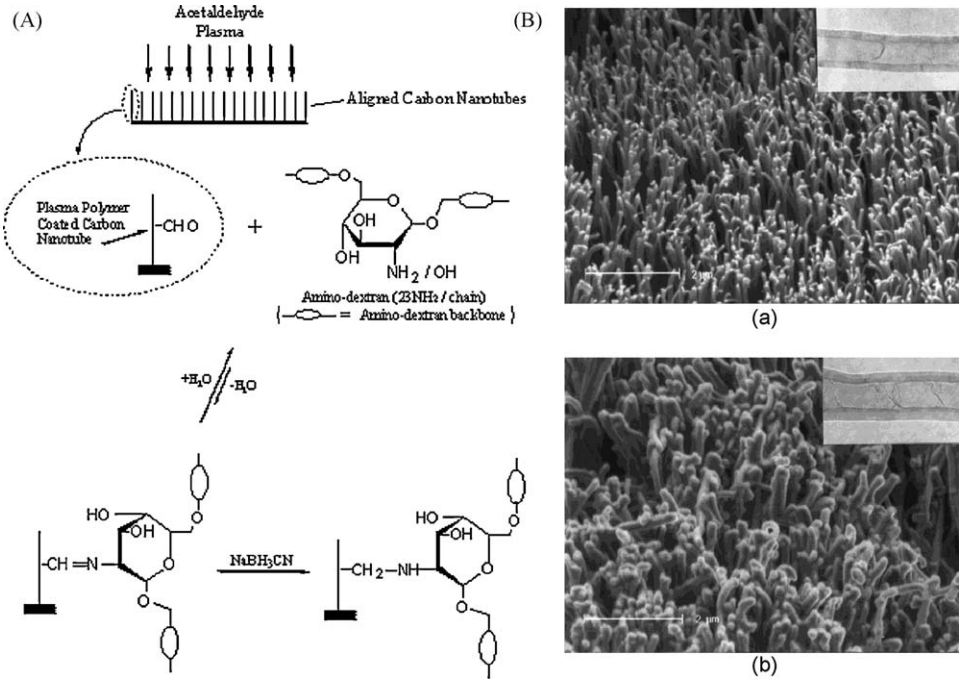

Fig. 20. (A) Schematic representation of grafting polysaccharide chains onto plasma activated aligned CNTs through Schiff-base formation, followed by reductive stabilization of the Schiff-base linkage with sodium cyanoborohydride. (B) SEM images of the VA-CNTs (a) before and (b) after the plasma polymerization of acetaldehyde. The insets show TEM images of an individual nanotube (a) before and (b) after being coated with a layer of the acetaldehyde-plasma-polymer. Note that the micrographs shown in (a) and (b) were not taken from the same spot due to technical difficulties (adapted from Ref. [189]).

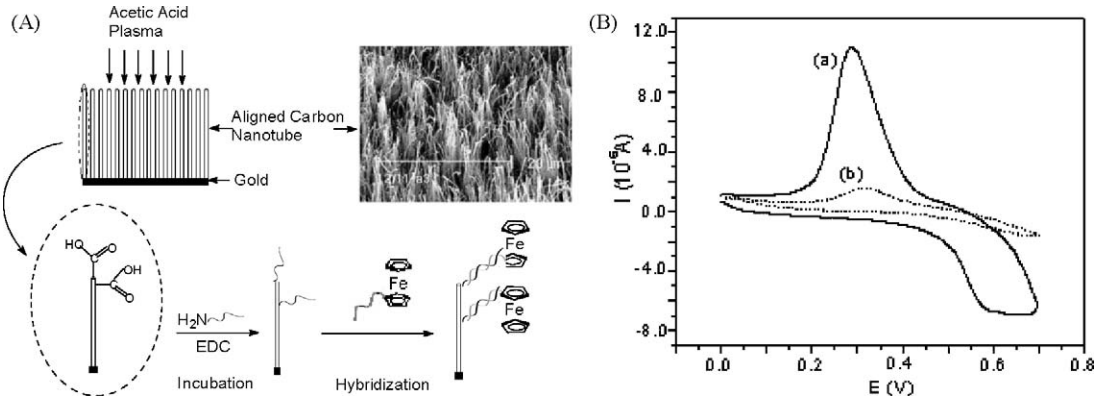

Fig. 21. (A) A schematic illustration of the aligned nanotube-DNA electrochemical sensor. The up-right SEM image shows the aligned CNTs after having been transferred onto a gold foil. For reasons of clarity, only one of the many carboxyl groups is shown at the nanotube tip and wall, respectively. (B) Cyclic voltammograms of (a) the aligned carbon nanotube electrode immobilized with ssDNA chains followed by hybridization with the FCA-labeled cDNA probes and (b) an Au electrode immobilized with ssDNA chains followed by hybridization with the FCA-labeled cDNA probes under the same conditions. The electrochemical measurements were carried out in an aqueous solution of 0.1 M H_2SO_4 *vs.* Ag/AgCl at a scan rate of 0.1 V s^{-1}. The concentration of the FCA-labeled cDNA probe is 0.05 mg mL^{-1} (adapted from Ref. [190]).

rather harsh conditions involved, however, most of the above conventional solution reactions caused the uncontrolled opening of the nanotube tips or detrimental damage to their sidewalls, or both. Simple application of the solution chemistry to VA-CNTs can thus damage the alignment and/or the nanotube structure. To chemically modify VA-CNTs while largely retaining their structural integrity, Chen et al. [189] have developed a novel approach for chemical modification of VA-CNTs by carrying out RFGD plasma treatment, and subsequent reactions characteristic of the plasma-induced surface groups. In particular, they have reported the surface immobilization of polysaccharide chains onto acetaldehyde-plasma-polymer-coated VA-CNTs through the Schiff-base formation, followed by reductive stabilization of the Schiff-base linkage with sodium cyanoborohydride (Fig. 20). Being very hydrophilic and biocompatible, the surface-bound polysaccharides provide highly hydrated coatings with important implications for using the modified CNTs in biological systems.

The aligned nature of the VA-CNTs can not only facilitate chemical modification of VA-CNTs but also the development of nanotube nanodevices (*e.g.* sensors and sensor arrays). For instance, He and Dai [190] have used an acetic acid plasma to activate the VA-CNTs generated from pyrolysis of FePc [67,191,192] for grafting single-strand DNA (ssDNA) chains with an amine group at the 5′-phosphate end (*i.e.* [AmC6]TTGACACCA-GACCAACTGGT-3′) through the amide formation in the presence of EDC coupling reagent (Fig. 21A). Complementary DNA (cDNA) chains pre-labeled with ferrocennecarboxaldehyde, FCA, (designated as: [FCA-C6]ACCA-GTTGGTCTGGTGTCAA-3′) were then used for hybridizing the surface-immobilized oligonucleotides to form double strand DNA (dsDNA) helices on the VA-CNT electrodes

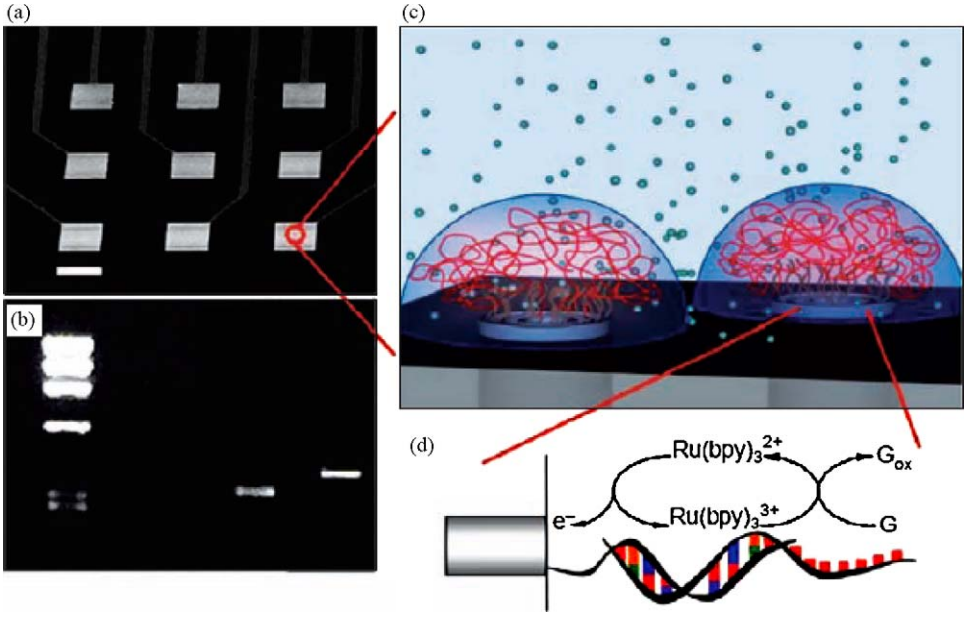

Fig. 22. (a) SEM image of an individually addressable 3 × 3 VA-MWNT microcontact array (scale bar, 200 μm). (b) Gel electrophoresis. The lanes (migration lines of DNA samples through agarose gel) from left to right are DNA molecular-weight standard (ΦX174RFDNAHaeIII digest), a specific polymerase chain reaction (PCR) amplicon target with ~300 bases, and a control sample with an unrelated PCR amplicon with ~400 bases, respectively. PCR enables researchers to produce millions of copies of a specific DNA sequence in approximately two hours. Gel electrophoresis is a DNA separation method that uses electricity to separate DNA fragments by size as they migrate through a gel matrix. The bright lights indicate the separated DNA fragments. (c) Schematic representation of the mechanism to detect DNA hybridization using a MWNT nanoelectrode array. The long single-stranded DNA PCR amplicons are hybridized to the short oligonucleotide probes, which are functionalized at the very end of the MWNTs. $Ru(bpy)_3^{2+}$ mediators are used to transfer electrons from the guanine groups to the MWNT nanoelectrode for all target molecules within the hemispherical diffusion layer of the nanoelectrodes. (d) The schematic mechanism for the guanine oxidation amplified with $Ru(bpy)_3^{2+}$ mediators (adapted from Ref. [204]).

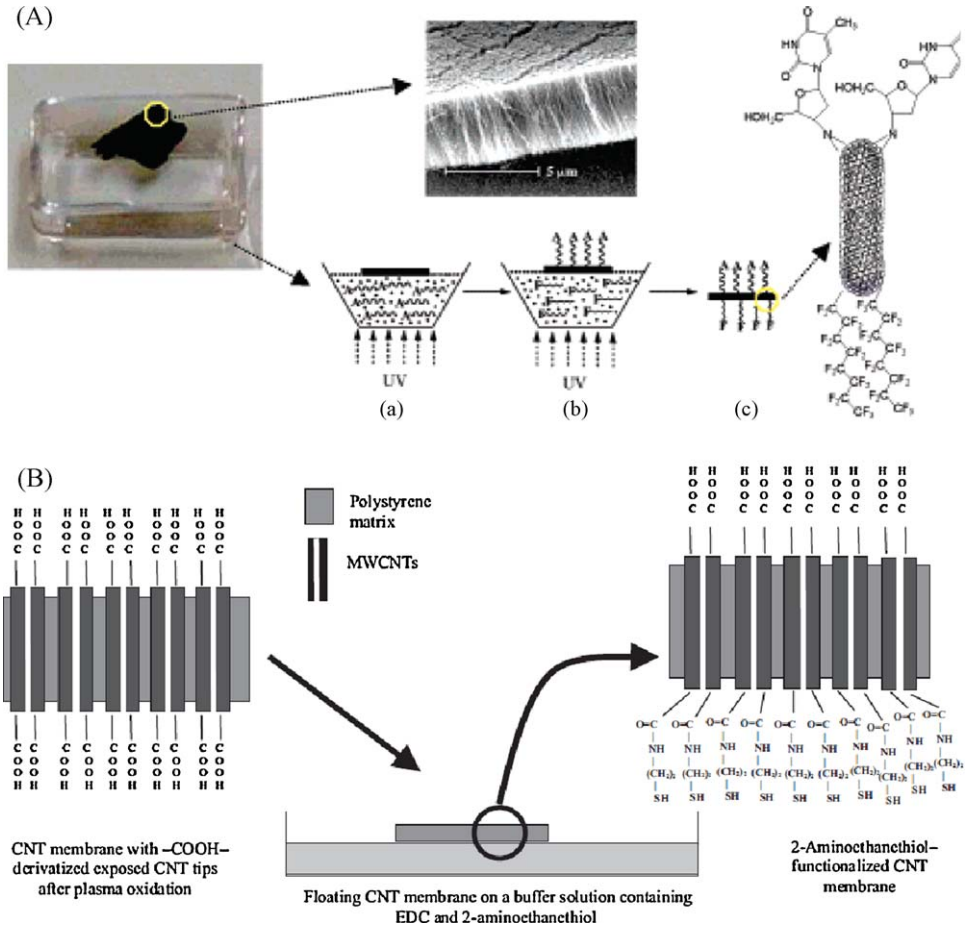

Fig. 23. (A) A free-standing film of VA-CNTs floating on the top surface of (a) a 3′-azido-3′-deoxythymidine solution in ethanol (2%) for UV irradiation at one side of the nanotube film for 1 h, and (b) a perfluorooctyl iodide solution in 1,1,2,2-tetrachloroethane (2%) for UV irradiation at the opposite side of the nanotube film for 1.5 h (adapted from Ref. [210]). (B) Plasma-oxidized VA-MWNT membrane (cross-sectional view) with carboxylic acid-derivatized MWNTs when floated on a buffer solution containing EDC and 2-aminoethanethiol, leading to bifunctional CNTs in the membrane structure (adapted from Ref. [211]).

(Fig. 21A), leading to highly reversible electrochemical signals arising from the hybridization and denaturing processes (Fig. 21B) [190]. This work demonstrated a concept for the development of vertically-aligned CNT-DNA sensors for probing complementary DNA chains of different base sequences with a high sensitivity and selectivity [193–195]. The ability to graft plasma-activated CNTs with DNA chains provides greater scope for not only the attachment of the additional components onto the nanotube structure, but also the self-assembly of the modified CNTs into useful supermolecular structures [196].

Along with the above-mentioned plasma activation and coating of nanoscale materials [197], plasma etching [198,199] has also been used to open the VA-CNT tips for membrane [200–202] and energy-related applications [203] to be described later. Besides, Koehne and Meyyappan [204] have developed more advanced micropatterned ultrasensitive DNA biosensors from aligned and micropatterned CNT electrodes (Fig. 22). CNT-based flow sensors may also be developed for sequence-dependent separation and sensing of certain biological species, including nucleic acids [201,205,206].

The use of carbon nanotubes for many practical applications often requires a precision loading of individual nanotubes into various functional structures and devices. The synthesis of aligned and/or micropatterned carbon nanotubes described above has played a critical role in facilitating the integration of carbon nanotubes into certain useful devices (*e.g.* electron emitters, transistors). However, a more general self-assembling approach would allow the construction of individual nanotubes into various functional structures with a molecular precision. For this purpose, the site-selective chemical modification of carbon nanotubes is essential. Recent work on selective modification of carbon nanotube tips, inner walls, and/or outer walls has opened a rich field of carbon nanotube chemistry [38,39,207–209].

To achieve the asymmetric end-functionalization of carbon nanotubes with a molecular level control, Lee et al. [210] have developed a simple but effective photochemical approach to directly grafting different chemical reagents onto the opposite tube-ends of individual CNTs. This was done by sequentially floating a substrate-free VA-CNT film on two different photoreactive solutions with only one side of the VA-CNT film being contacted with a photoreactive solution for UV-induced functionalization each time, as schematically shown in Fig. 23A [210]. In a similar but independent study, asymmetric end-functionalization of CNTs has also been achieved through sidewall protection by impregnating a VA-MWNT array with polystyrene [211], as schematically shown in Fig. 23B. These methodologies could be used to asymmetrically end-functionalize CNTs with ssDNA and cDNA chains onto their opposite tube-ends, which should be very useful for site-selective self-assembly of the asymmetrically end-functionalized CNTs into many novel functional structures.

3.2. Modification of VA-CNTs by electrochemical deposition

In addition to the plasma and photochemical activation, Gao et al. [212] have used VA-CNTs as nanoelectrodes for making conducting coaxial nanowires by electrochemically depositing a

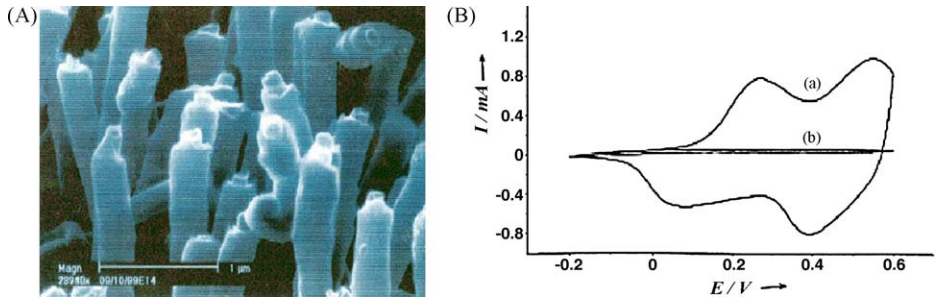

Fig. 24. (A) Typical SEM images of the CP-NT coaxial nanowires produced by cyclic voltammetry on the VA-CNT electrode, showing a thin layer of conducting polymer (polypyrrole) coating surrounding each of the constituent aligned CNTs. (B) Cyclic voltammograms of (a) the polyaniline-coated CP-NT coaxial nanowires and (b) the bare VA-CNTs. Measured in an aqueous solution of 1 M H_2SO_4 with a scan rate of 50 mV/s (adapted from Ref [212]).

concentric layer of an appropriate conducting polymer uniformly onto each of the constituent aligned nanotubes to form the vertically-aligned conducting polymer coated CNT coaxial nanowires (CP-NT) (Fig. 24A).

The electrochemical performance of the aligned CP-NT coaxial nanowires was evaluated by carrying out cyclic voltammetry measurements. As for polyaniline films electrochemically deposited on conventional electrodes, the cyclic voltammetric response of the polyaniline coated nanotube array in an aqueous solution of 1 M H_2SO_4 (Fig. 24B(a)) shows oxidation peaks at 0.33 and 0.52 V (but with much higher current densities) [213]. This indicates that polyaniline films thus prepared are highly electroactive. As a control, the cyclic voltammetry measurement was also carried out on the bare aligned nanotubes under the same conditions (Fig. 24B(b)). In the control experiment, only capacitive current was observed with no peak attributable to the presence of any redoxactive species. The potential sensing applications for the vertically-aligned CP-CNT coaxial nanowires have also been demonstrated [194]. Macroscopic coaxial carbon cylinders (~0.5 cm in diameter with varying length, ~7–10 cm) consisting of VA-CNT stacks have been prepared by controlled spray pyrolysis [214]. Enhanced electrical conductivity and mechanical strength were observed for the resultant nanotube and polymer composites (*e.g.* polyethylene oxide, polyacrylamide). The coaxial structure should allow the nanotube framework to provide a good mechanical stability, high thermal/electrical conductivity, and large surface/interface area necessary for efficient optoelectronic and sensing devices. The alignment structure will also allow the constituent nanotube devices to be collectively addressed through a common substrate/electrode.

The large surface area, good chemical/mechanical stability, and excellent electronic property also make carbon nanotubes, particularly VA-CNTs, very useful for supporting metal nanoparticles for many potential applications, ranging from advanced catalytic systems, through very sensitive electrochemical sensors, to highly efficient fuel cells [215,216]. Consequently, functionalization of carbon nanotubes with metal nanoparticles has received increasing interest in recent years, and some interesting routes have been devised for either covalently or noncovalently attaching metal nanoparticles onto carbon nanotubes [217–222]. Among them, the electroless deposition is of particular interest because its simplicity could facilitate large-scale production of the nanotube-nanoparticle hybrids at low cost. General applications of the electroless deposition, however, are limited by the fact that only metal ions of a redox potential higher than that of a reducing agent or carbon nanotube can be reduced into nanoparticles on the nanotube support. By simply supporting carbon nanotubes with a metal substrate of a redox potential lower than that of the metal ions to be reduced into nanoparticles, Qu and Dai [223] have recently developed a facile yet versatile and effective substrate-enhanced electroless deposition (SEED) method for decorating CNTs with various metal nanoparticles, including those that cannot

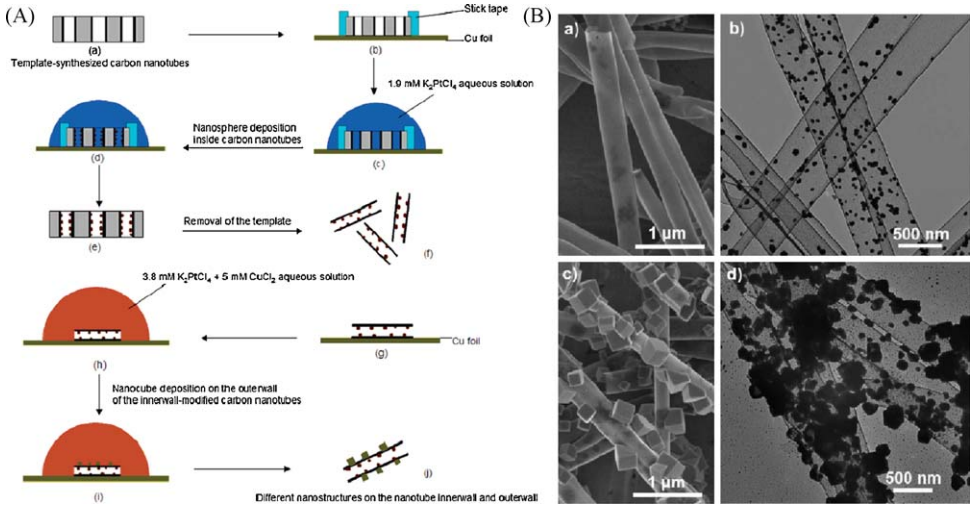

Fig. 25. (A) Procedures for the CNT innerwall modification and the asymmetric modification of the nanotube innerwall with Pt nanospheres and the outerwall with nanocubes. (B) (a) SEM and (b) TEM images of CNTs having their innerwall modified with Pt nanospheres. (c) SEM and (d) TEM images of the innerwall-modified CNTs followed by outerwall modification in an aqueous solution of K_2PtCl_4 containing $CuCl_2$ with the innerwall-modified CNTs being supported by a Cu foil in a sidewall-on configuration (adapted from Ref. [224]).

be made by more conventional electroless deposition methods, in the absence of any additional reducing agent [223,224]. Using this approach, Qu and Dai [223] have deposited Cu, Ag, Au, Pt and Pd nanoparticles onto SWNTs and MWNTs. In conjugation with VA-CNTs, asymmetric sidewall modification by attaching the inner-wall and outerwall of CNTs with metal nanoparticles of different shapes was also achieved. As shown in Fig. 25A, VA-CNTs were first deposited into a commercially available alumina membrane (Fig. 25A(a)). Then Pt nanospheres were deposited onto the innerwall of the *template-synthesized* VA-CNTs supported by a Cu foil (Fig. 25A(b–e)), in which the template acts as a protective layer for the nanotube outerwall. Upon the completion of the innerwall modification, the innerwall-modified nanotubes were released by dissolving the alumina template in aqueous HF (Fig. 25A(f)). As expected, Fig. 25B(a and b) shows a very smooth outerwall for the innerwall modified CNTs. The presence of nanospheres within the nanotube innerwall was clearly seen in Fig. 25B(b). To deposit Pt nanocubes onto the outerwall, the innerwall-modified CNTs were supported in a sidewall-on configuration (Fig. 25A(g–j)) on a Cu foil and exposed to an aqueous K_2PtCl_4 solution containing $CuCl_2$ for 1 min. While Fig. 25B(c) clearly shows the presence of nanocubes on the nanotube outerwall, Fig. 25B(d) reveals the asymmetrically modified CNTs with nanocubes and nanospheres deposited onto the nanotube outerwall and innerwall, respectively.

Using electrophoresis for titanium dioxide (TiO_2) coating and photoexicited electrons for metal nanoparticle deposition, Yang et al. [225] have also developed a facile yet versatile and effective method for the development of aligned coaxial nanowires of CNTs sheathed with titanium dioxide (TiO_2), and well-defined TiO_2 nanomembranes decorated with and without metal nanoparticles. Fig. 26a shows a typical SEM image of the VA-CNTs of *ca.* 7 μm long. The corresponding SEM image under a higher magnification in Fig. 26b shows an average diameter of *ca.* 50 nm for the as-synthesized CNTs. Upon electrophoresis, TiO_2 clusters were deposited on sidewalls of the VA-CNTs as nanoparticles (Fig. 26c). Further electrophoresis deposition up to approximately 30 min caused additional TiO_2 clusters to fill up the spaces between the pre-deposited TiO_2 nanoparticles, leading to the growth of a continuous TiO_2 coating along the whole nanotube length (Fig. 26d). Fig. 26d shows similar features as the pristine VA-CNTs (Fig. 26b) but with a larger diameter (*ca.* 120 nm on average) due to the presence of the newly-coated TiO_2 layer.

A top-view SEM image of the sample in Fig. 26d after the heat treatment at 600 °C in air for 30 min was given in Fig. 26e, which clearly shows the vertically-aligned coaxial nanowires of CNTs sheathed with TiO_2 coating with some of the CNT cores having been removed by oxidation with air under the high temperature. Fig. 26f shows a typical TEM image taken at the tip region of the vertically-aligned CNT-TiO_2 coaxial nanowires, showing a poly-crystalline (Inset of Fig. 26f) TiO_2 coating along the nanotube length. The thickness of the TiO_2 layer was determined from the TEM image to be approximately 30–40 nm, consistent with the SEM observation (*cf.* Fig. 26(b and d)). By annealing the sample corresponding to Fig. 26e at 600 °C in air for 2 h, most of the VA-CNT templates were removed through air oxidation, leaving the TiO_2 hollow shells as aligned TiO_2 nanotubes (Fig. 26g). Prolonged electrophoretic deposition led to partially or fully infiltrating TiO_2 into the gaps between the constituent vertically-aligned CNT-TiO_2 coaxial nanowires, as exemplified by Fig. 8h. Thermal annealing the partially or fully TiO_2-infiltrated VA-CNT films resulted in the formation of either a loosely-packed (Fig. 26i) or more densely-packed (Fig. 26j) TiO_2 membrane. Raman spectroscopic measurements and XRD diffraction on the TiO_2-coated VA-CNT sample corresponding to Fig. 26e shows a TiO_2 anatase phase [226].

The anatase phase of TiO_2 has a band gap of approximately 3.2 eV, which could be considered as a wide band gap photo-electronically active semiconductor. Indeed, TiO_2 has been widely used as a class of photocatalysts for environment protection by decomposing organisms with UV irradiation. Therefore, these vertically-aligned CNT-TiO_2 coaxial nanowires, TiO_2 nanotubes, and TiO_2 nanomembranes showed very fast photocurrent responses to a pulsed light beam (λ = 254 nm, 4 W) with a good repeatability (Fig. 27). The observed photocurrent response allowed for the use of the photoexcited electrons from TiO_2 to deposit various metal nanoparticles (*e.g.* Au, Ag, Pd, Pt) onto the TiO_2 nanostructures without involving any reducing agent, as in the case for deposition of metal nanoparticles onto CNT structures by the aforementioned SEED method [223,224]. Similar coaxial structures of VA-CNTs sheathed with indium tin oxide (ITO) thin film have also been produced by ion-assisted sputter-coating [227]. The resultant hybrid nanomaterials are expected to be useful in solar cells, flexible electronics and displays.

3.3. Modification of VA-CNTs by chemical functionalization and doping

The aligned CNT structure can also be well preserved via direct chemical polymerization of monomer or selectively etching in liquid phase with appropriate protection. Feng et al. [228] reported the preparation of vertically-aligned coaxial polyaniline (PANI)-CNTs by *in situ* polymerization. The VA-CNTs were dipped in aniline/HCl solution, which led to the adsorption aniline monomer on the surface of CNT (Fig. 28a and b). A solution of ammonium peroxydisulfate dissolved in HCl was added dropwise to initiate the *in situ* polymerization of aniline monomer around the VA-CNTs (Fig. 28c and d). *In situ* polymerization by infiltrating monomer molecules into the VA-CNT arrays was also reported [229,230].

On the other hand, the aligned CNTs can also be treated by acid solution to generate chemical functional groups at opened ends of the CNT. As mentioned earlier, Meyyappan and co-workers [231] developed an effective method for protecting the alignment structure by filling the gaps between the aligned nanotubes with a spin-on glass (SOG) prior to the oxidative reaction. Fig. 29A shows a schematic representation of the fabrication and pretreatment of the aligned carbon nanotubes for further functionalization [231], whilst Fig. 29B reveals the oxidation-induced changes in alignment for the VA-CNTs with and without the SOG protection. Compared to Fig. 29B(b), Fig. 29B(c) indicates that the SOG film provides structural support to the aligned carbon nanotubes. After having successfully functionalized the tips of the VA-CNTs with carboxy groups, these authors further demonstrated accomplishments in chemical coupling of nucleic acids to the aligned nanotube array using the standard water soluble coupling reagents (*i.e.* EDC and *N*-hydroxysulfosuccinimide, sulfo-NHS), as schematically shown in Fig. 29C.

Chemical doping is another approach that can be used to functionalize VA-CNTs at atomic scale [232–236], which introduces additional electronic states around the Fermi level. Thus, doped-CNTs are attractive for enhanced electron emission, charge storage, and other nanoelectronic devices [232–238]. Gong et al. [239] have recently found that vertically aligned nitrogen-containing CNTs (VA-NCNTs) produced by pyrolysis of FePc [67], in either the presence or absence of additional NH_3 vapor [240], could act as extremely effective metal-free electrocatalysts for oxygen reduction reaction (ORR) (Fig. 30). The ORR at the cathode of fuel cells plays a key role in controlling the performance of a fuel cell, and efficient ORR electrocatalysts are essential for practical applications of the fuel cells [241]. The ORR at cathode, when coupled with oxidation on the anode, produces water as the end product, leading to the direct conversion of chemical energy into electricity. Alkaline fuel cells with platinum-loaded carbon as an electrocatalyst for the four-electron ORR were developed for the

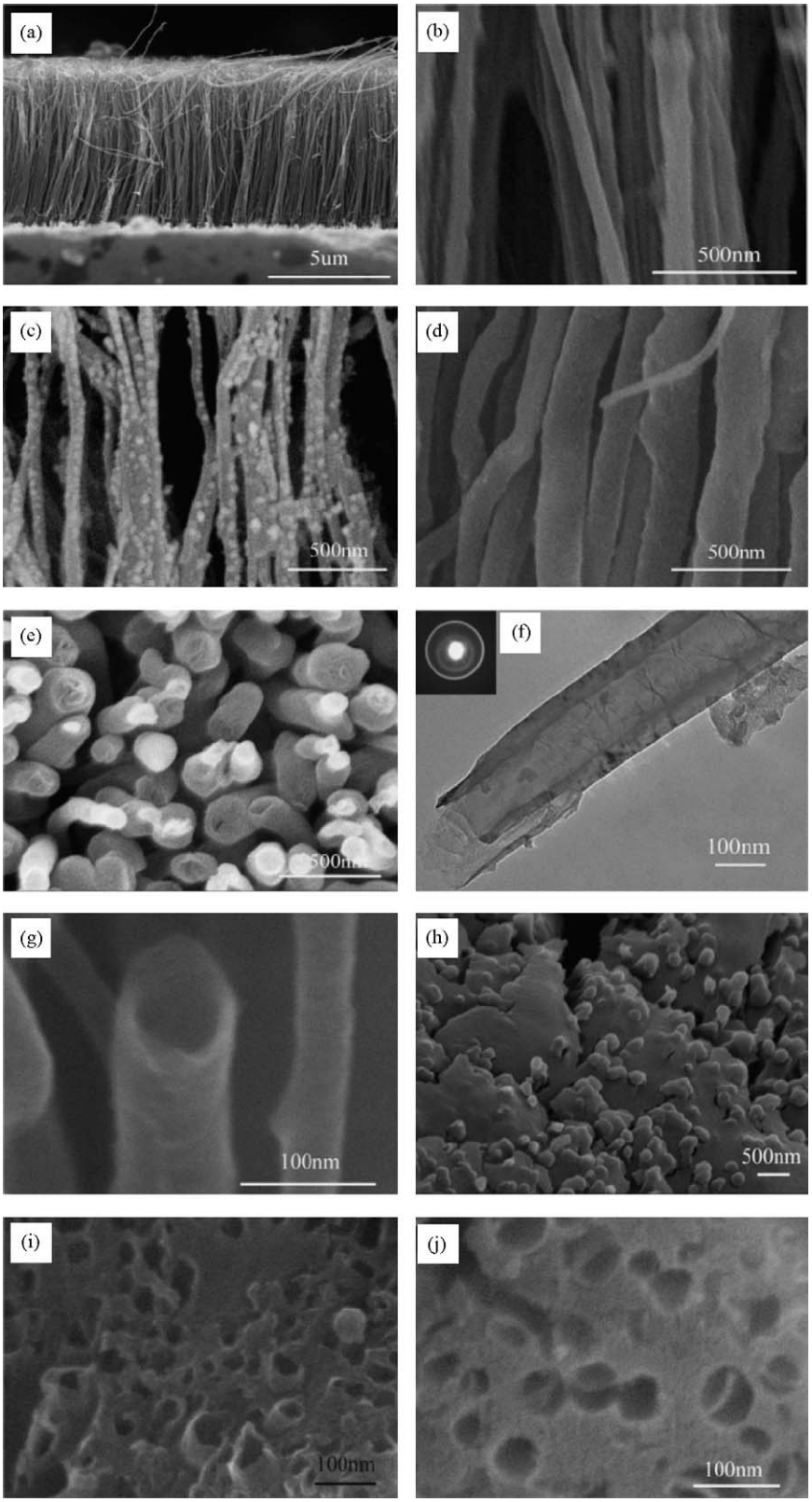

Fig. 26. SEM images of (a) the VA-CNTs (The misalignment seen for some of the CNTs was caused by the nanotube electrode preparation), (b) as for (a) under a higher magnification. The corresponding SEM images for the VA-CNTs after the electrophoresis deposition of TiO_2 coating at 1 V at different deposition times: (c) 15 min, (d) 30 min, and (e) top-view of the vertically-aligned CNT-TiO_2 coaxial nanowires corresponding to (d) after the heat treatment at 600 °C in air for 30 min, which has been turned over from the Si substrate to demonstrate the possibility of transferring the aligned nanowire array with full integrity. (f) A TEM image of the resultant TiO_2-coated VA-CNTs shown in (d). Inset of (f) shows an electron diffraction pattern of the TiO_2 coating. SEM images of (g) the sample corresponding to (e) after thermal annealing at 600 °C in air for 2 h, showing vertically-aligned TiO_2 hollow tubes after the removal of the VA-CNT template through air oxidation, (h) VA-CNTs after a prolonged electrophoretic coating with TiO_2 at 1 V for 3 h, and (i, j) the loosely and more densely packed TiO_2 membranes formed by annealing the corresponding TiO_2-infiltrated VA-CNT films at 600 °C in air for 2 h (adapted from Ref. [225]).

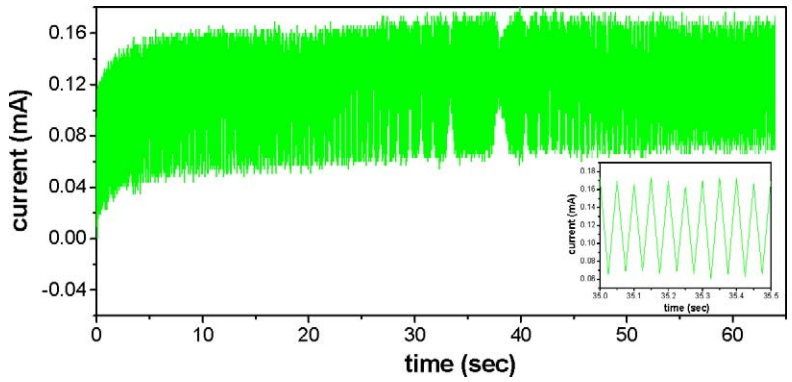

Fig. 27. A typical photocurrent response for a vertically-aligned CNT-TiO_2 coaxial nanowire film under UV exposure (λ = 254 nm, 4 W) at room temperature. Inset shows an enlarged view for a small portion of the photocurrent response curve. The sample size is approximately 1 cm^2 (adapted from Ref. [225]).

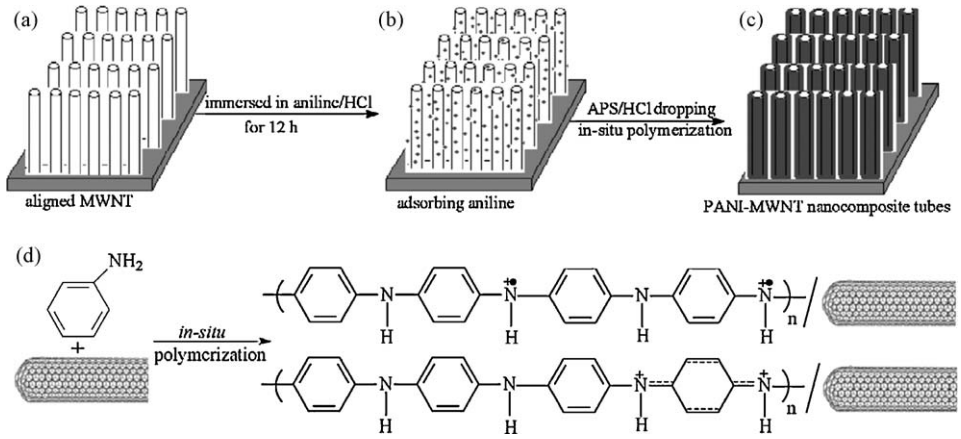

Fig. 28. Preparation procedures for coating VA-CNTs with PANI by *in situ* polymerization: (a) VA-MWNT film grown on a quartz substrate by catalytic pyrolysis. (b) The VA-MWNT film was immersed into aniline/HCl solution at 0.8 °C for 12 h. (c) *In situ* polymerization of aniline around the MWNT surface. (d) Reaction mechanism for polymerization of aniline around CNTs (adapted from Ref. [228]).

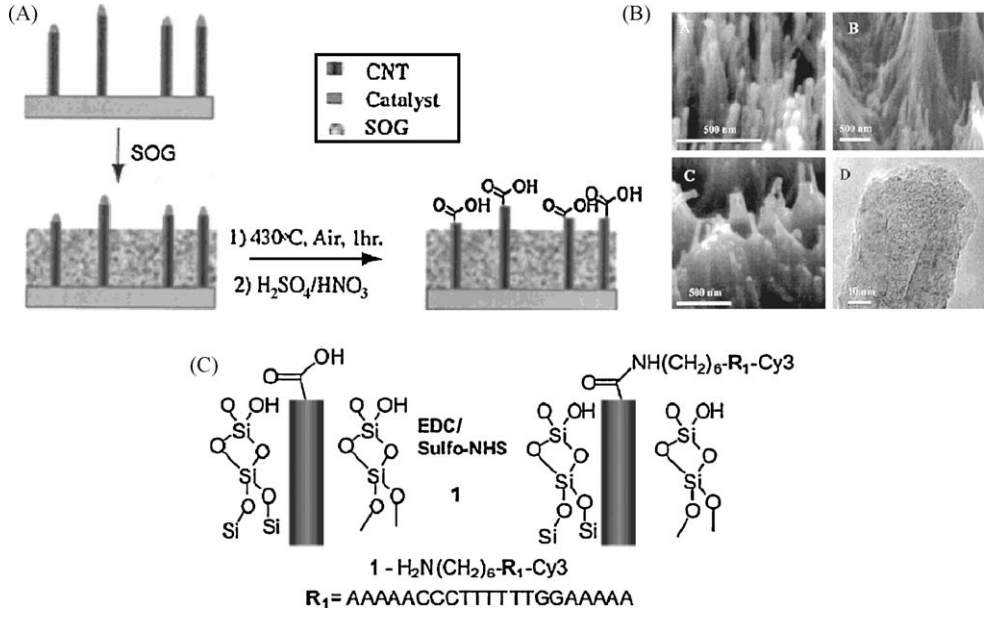

Fig. 29. (A) Schematic representation of the fabrication and pretreatment of the aligned carbon nanotubes for further functionalization. (B) SEM images of (a) VA-CNT arrays; (b) the collapsed carbon nanotube array without SOG after the oxidative treatment; and (c) the aligned carbon nanotube array with SOG after the oxidative treatment. (d) High-resolution TEM image of the opened carbon nanotube. (C) Reaction scheme for chemical coupling of nucleic acids to the VA-CNTs (adapted from Ref. [231]).

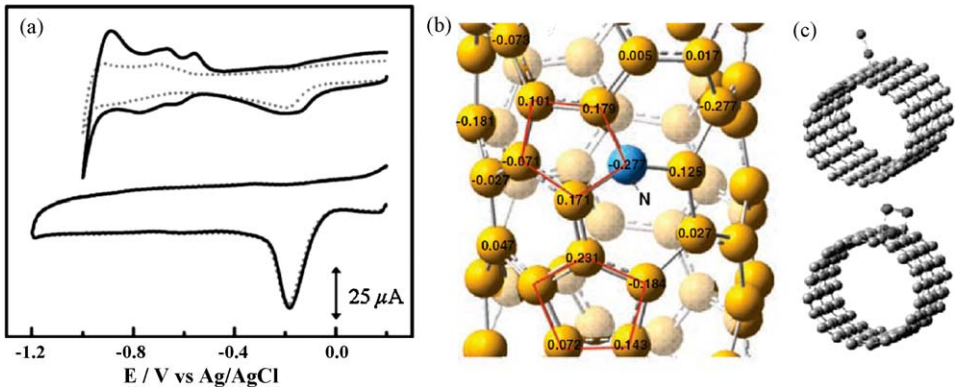

Fig. 30. (a) Cyclic voltammograms for the ORR at the Pt-C/GC (top) and aligned NCNT/GC (bottom) electrodes before (solid black curves) and after (dotted curves) a continuous potentiodynamic swept for ~100,000 cycles. (b) Calculated charge density distribution for the NCNTs. (c) Schematic representations of possible adsorption modes of an oxygen molecule at the CCNTs (top) and NCNTs (bottom) (adapted from Ref. [239]).

Apollo lunar mission in the 1960s [242], but their large-scale commercial application has been precluded by the high cost of the requisite noble metals. Apart from its high cost, the Pt-based electrode also suffers from its susceptibility to time dependent drift [243] and CO deactivation [244]. Recent research efforts focused on reducing or replacing Pt-based electrode in fuel cells have led to the development of new ORR electrocatalysts, including Pt-based alloys [245], carbon nanotube–supported metal particles [51,246,247], enzymatic electrocatalytic systems [248], and even conducting poly(3,4-ethylenedioxythiophene) (PEDOT)–coated membranes [249]. The metal-free VA-NCNTs were shown to catalyze a four-electron ORR process free from CO "poisoning" with a 3-time higher electrocatalytic activity, smaller crossover effect, and better long-term operation stability than that of commercially available platinum-based electrodes (C2-20, 20% platinumonVulcanXC-72R; E-TEK) in alkaline electrolytes [239]. A steady-state output potential of −80 millivolts and a current density of 4.1 milliamps per square centimeter at −0.22 volts, compared with −85 millivolts and 1.1 milliamps per square centimeter at −0.20 volts for a platinum-carbon electrode (Fig. 30a), have been obtained for the VA-NCNT electrode [239].

Based on the experimental observations and quantum mechanics calculations, the improved catalytic performance for VA-NCNTs has been attributed to the electron-accepting ability of the nitrogen atoms to create net positive charge on adjacent carbon atoms in the nitrogen-doped nanotube carbon plane for facilitating the ORR by readily attracting electrons from the anode [239]. The nitrogen-induced charge delocalization can also change the chemisorption mode of O_2 from the usual end-on adsorption at the CCNT surface (top, Fig. 30c) to a side-on adsorption onto the NCNT electrodes (bottom, Fig. 30c). The parallel diatomic adsorption could effectively weaken the O–O bonding to facilitate ORR at the NCNT/GC electrodes. As such, doping CNTs with nitrogen heteroatoms as in the NCNT electrodes can efficiently create the metal-free active sites for electrochemical reduction of O_2, and even new catalytic materials for applications beyond fuel cells.

3.4. Modification of VA-CNTs by polymer masking

CNTs have been widely investigated for their application as reinforcement fillers in polymer composites [2,4,250–252]. The ability to control their interaction with and orientation within polymer matrices is of paramount importance for tailoring the structure and property of the resultant nanocomposites [2,253–256]. The chemistry of CNTs has matured now for functionalizing nonaligned CNTs with various tailor-made surface characteristics to control their interaction with polymers and other materials [36,38,208,209,257,258]. In contrast, it is just a recent development to prepare polymer and VA-CNT composites of a controlled nanotube orientation in and interfacial interaction with the polymer matrix. A few recent studies have demonstrated that the embedment of VA-CNTs, either partially or fully, into appropriate polymer matrices generated important synergetic effects that provide novel concepts and new properties for multifunctional applications, ranging from advanced chemical and biological sensors [229,231,259–262], through smart membranes [200,201,263], to flexible electronics [264]. While several different matrix materials, including poly(dimethylsiloxane) (PDMS) [264], polystyrene (PS) [200,201], poly(methyl methacrylate) (PMMA) [229], spin-on-glass [231], and polydiene rubber [260], have been used for embedding VA-CNTs, solution-coating has remained as the main method to achieve the embedment. Although the solution-based approach provides an effective means for fully embedding VA-CNTs through the whole nanotube length, it could be a big challenge for the solution coating to control the nanotube length being embedded (designed as: the embedment length) into an appropriate matrix (*e.g.* polymer). By simply heating a polymer thin film on the top of a VA-CNT array, Qu and Dai [265] have demonstrated that the VA-CNTs can be embedded into the polymer matrix for any predetermined embedment length up to the whole nanotube length in a controllable fashion.

As schematically shown in Fig. 31A(a), an appropriate polymer thin film (*e.g.* PS; M_w = 350,000; T_g (glass transition temperature) ≈105 °C; T_m (melting point) ≈180 °C; T_c (decomposition temperature) ≈350 °C; thickness: ~50 μm) was first placed on the top surface of a VA-CNT array (Fig. 31A(a)). Upon heating the SiO_2/Si substrate by an underlying hot plate to a temperature above T_m and below T_c, the melted PS film gradually filtrated into the nanotube forest (Fig. 31A(a)) through a combined effect of the gravity and capillary forces. As expected, the infiltration depth (*i.e.* the embedment length) of PS into the nanotube forest depends strongly on the temperature and heating time. After a predetermined heating time, the polymer-infiltrated nanotube array was peeled off from the SiO_2/Si substrate in an aqueous solution of HF (10 wt%) to generate a free-standing film of VA-CNTs embedded into the PS matrix (Fig. 31A(a)). While Fig. 31A(b) shows a typical SEM image of the pristine VA-CNTs, Fig. 31A(c–g) reproduce SEM images of the VA-CNTs embedded into PS films after being heated at different temperatures for 1 min. For the given infiltration time of 1 min, the embedment length increased with the heating temperature from *ca.* 10% coverage of the nanotube length at 180 °C up to the full length coverage at 245 °C (Fig. 31A(c–g)). A more quantitative relationship between the embedment length

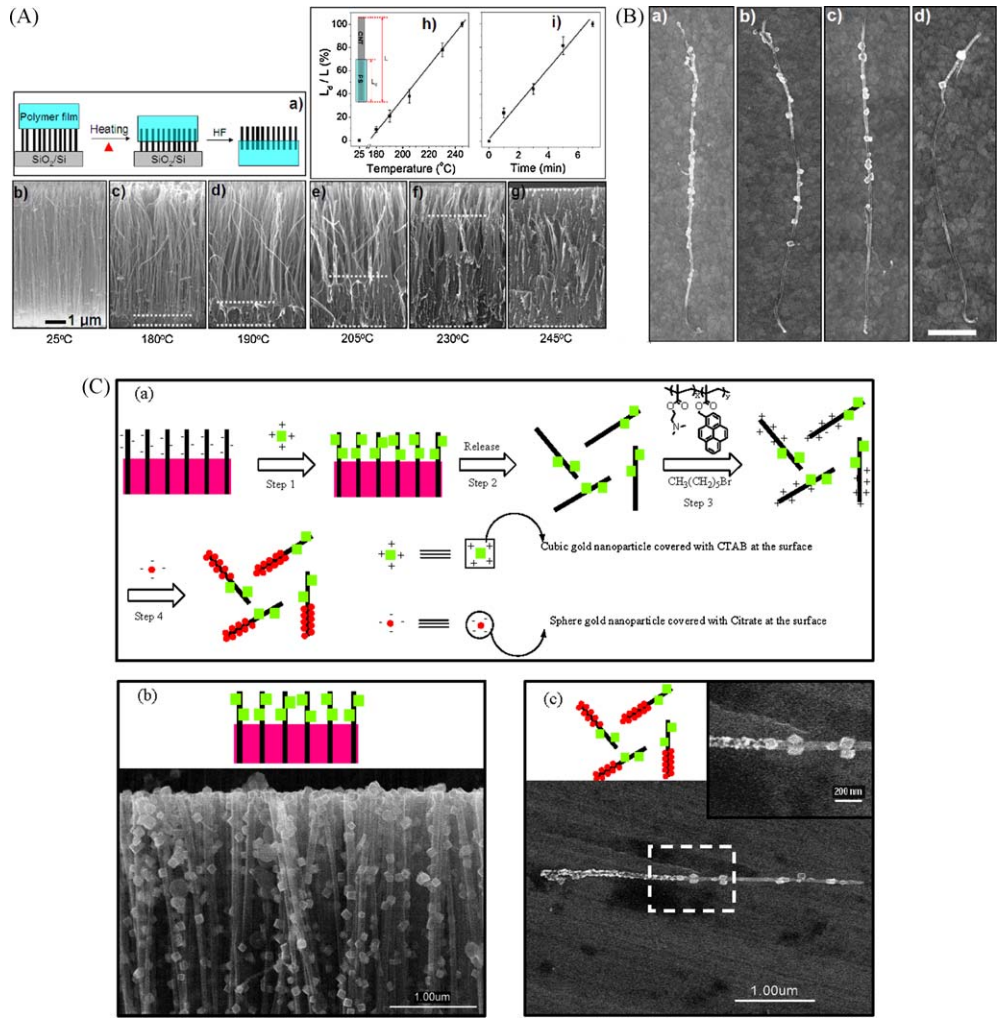

Fig. 31. (A) (a) Schematic representation of the VA-CNTs embeded into a polymer matrix by thermal infiltrating the melted polymer into the nanotube forest; (b–g) SEM images of (b) the pristine VA-CNT array and (c–g) the VA-CNT array after being embedded into PS films by heating at different temperatures for 1 min. The dashed-line gaps crossing the polymer coated regions show the approximate embedment length for each of the PS-embedded VA-CNTs; (h, i) temperature and time dependence of the embedment length for VA-CNTs embedded into the PS matrix (L: the nanotube length (~6 μm), L_d: the embedment length, which was estimated from the distance between the two dashed lines in each of the images shown in (c–g). (B) SEM images of individual CNTs released out from the PS-embedded VA-CNTs by THF washing after the Au nanoparticle deposition by SEED. (a–d) correspond to samples (c–f) in (A), respectively. Scale bar: 1 μm (adapted from Ref. [265]). (C) Asymmetric functionalization of CNTs with opposite charges. (a) A schematic representation of procedures for asymmetric functionalization of CNTs with opposite charges, followed by tube-length-specific deposition of gold nanoparticles via electrostatical interactions; (b) a schematic representation and SEM image of the CNT array partially functionalized with cubic gold nanoparticles; and (c) a schematic representation and SEM image of the resultant asymmetrically sidewall-functionalized CNTs with half of the nanotube length covered by gold nanocubes and the other half by spherical gold nanoparticles through electrostatical assembly (Inset shows a higher magnification SEM image for the squared area). Scale bars (b, c): 1 μm; Scale bar (right inset of c): 200 nm (adapted from Ref. [266]).

and the heating temperature is given in Fig. 31A(h), which shows a pseudo-linear relationship over a wide temperature range. For a given heating temperature (*e.g.* 195 °C), the embedment length was found to be directly proportional to the PS filtration time (*i.e.* heating time), as exemplified by Fig. 31A(i). These results clearly show the feasibility for the tube-length-specific functionalization of CNTs through the controllable embedment of VA-CNTs into the polymer matrix. This is because the portion of the nanotube sidewall embedded into the polymer matrix is physically masked whereas the polymer-free sidewall surface along the nanotube length can be selectively functionalized via various physicochemical processes.

In view of the ease with which shape/size-controlled metal nanoparticles can be deposited onto CNT structures by the aforementioned SEED method [223,224] and the effective action of the deposited nanoparticles as labeling centers for characterization, Qu et al. [265] have demonstrated the tube-length-specific functionalization of CNTs by SEED deposition of Au nanoparticles onto each of the VA-CNTs partially embedded into the PS matrices shown in Fig. 31A(c–f) at the polymer-free region along their sidewalls. Thereafter, the polymer support was washed off with THF to yield individual nanotubes region-selectively attached with the Au-nanoparticles, as shown in Fig. 31B. The portions of the nanotube length covered by the Au nanoparticles seen in Fig. 31B(a–d) consist with the corresponding nanotube lengthes extending out from the polymer matrices shown in Fig. 31A(c–f), respectively. This indicates that the polymer-masking technique can be effectively used to precisely control the portion(s) of the CNT length to be functionalized.

The polymer-masking approach has been used not only for asymmetrically functionalizing nanotube sidewalls by sequentially masking VA-CNTs twice with only half of the nanotube sidewall being modified each time, as exemplified in Fig. 31C [266], but also for imparting magnetic properties to CNTs simply by region-selectively sputter-coating a thin layer of magnetic material (*e.g.* iron) onto the top-tips of VA-CNTs embedded into a polymer

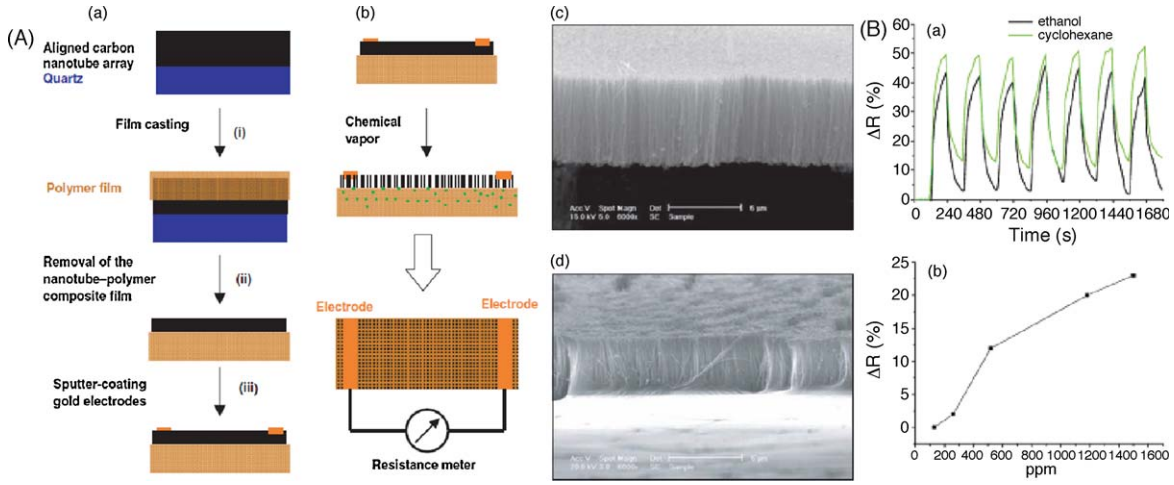

Fig. 32. (A) Schematic illustration for (a) fabricating and (b) characterizing the VA-CNT-polymer composite chemical vapor sensors. SEM images of the VA-MWNTs (c) before and (d) after being partially coated with a polymer (PVAc) film on top and turned upside down (Scale bars: 5 μm). (B) ΔR for a vertically-aligned CNT-PVAc/PI film during (a) cyclohexane-air and ethanol-air cycles, and (b) its equilibrium resistance peak height versus the partial cyclohexane vapor pressure (adapted from Ref. [259]).

matrix (*e.g.* PS film). Therefore, this polymer-masking approach, together with those functionalization methods mentioned above, should allow for the functionalization of VA-CNTs in a region-specific fashion with various reagents (*e.g.* ssDNA chains of specific sequences) for developing a wide range of novel nanotube-based multifunctional materials and devices.

By partially coating VA-CNT arrays with an appropriate polymer thin film along their tube length, sensors of a high sensitivity, good selectivity, and excellent environmental stability for the detection of a broad class of chemical vapors with low power consumption have also been developed [259]. The discovery of the gas sensing capabilities of nonaligned CNTs through the charge transfer or capacitance change by gas absorption (*e.g.* NH_3, NO_2, O_2) [142,262,267–271] is significantly intriguing as their small size, high surface area, good environmental stability, and excellent mechanical and electronic properties can offer many advantages for sensing applications [142,272,273]. However, it could be a significant advancement if *perpendicularly-aligned* carbon nanotube arrays can be used as the sensing materials because VA-CNTs, in either a patterned or nonpatterned form, allow the development of novel sensors and/or sensor chips without the need for direct manipulation of individual nanotubes since the constituent nanotubes can be *collectively* addressed through a common substrate/electrode [5,132,262]. The aligned nanotube structure further provides a large well-defined surface area and the capacity for modifying the carbon nanotube surface with various transduction materials [5,132,262] to effectively enhance the sensitivity and to broaden the scope of analytes to be detected. As schematically shown in Fig. 32A, the absorption and desorption of chemical vapors by the polymer matrix cause changes in the inter-tube distance, and hence the surface resistance changes across the nanotube film. Simple measurements of the resistance change, therefore, produce the sensor response. As can be seen in Fig. 32B, the chemical vapor sensors based on the aligned carbon nanotubes and poly(vinyl acetate)/polyisoprene (PVAc/PI) *binary* polymer composite show reasonably good responses to both cyclohexane and ethanol vapors (Fig. 32B(a)). The large-range good correlation between the equilibrium peak height for the resistance change and the partial cyclohexane vapor pressure shown in Fig. 32B(b) indicates a high sensitivity and reliability. The virtually unlimited number of combinations of VA-CNTs with different polymer systems should make this methodology highly versatile for developing various novel nanotube and polymer sensors for effectively detecting a large variety of chemical vapors. With appropriate surface modification for gaining specific interactions with analytes of biological significance [39,209], these polymer-supported VA-CNT sensors could also be used to detect biological systems in solution. These flexible composite films are also being developed for thermal, optical and mechanical sensors [259], and even dry adhesives mimicking gecko foot [76–80].

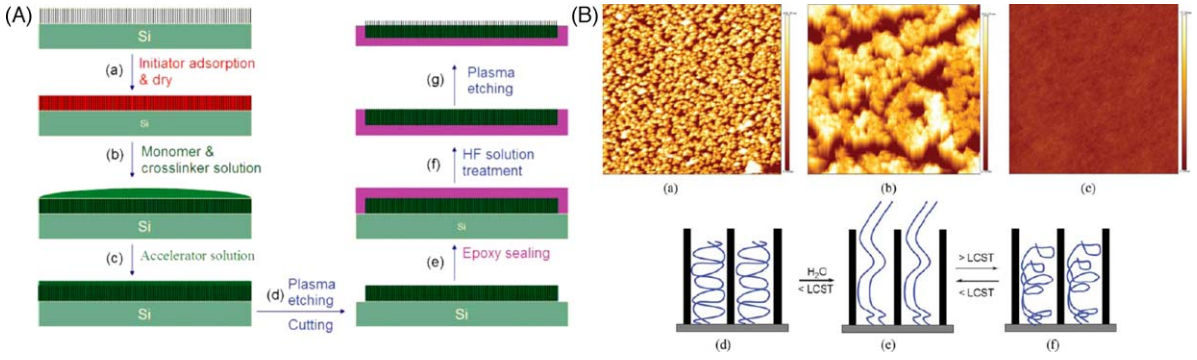

Fig. 33. (A) Illustration of the procedure for fabricating the smart PNIPAAm/VA-CNT nanocomposite films. (B) AFM images of (a) a pristine aligned CNT array and the PNIPAAm/VA-CNT nanocomposite film: (b) in the dry state and (c) in the wet state. *xy*-Scale: (a–c) 5 μm × 5 μm, *z*-scale: (a) 445 nm; (b) 667 nm. (c) 17 nm. A schematic representation of the PNIPAAm/VA-MWNT film: in the dry (d) and wet (e) state at room temperature (20 °C); and (f) in the wet state at a temperature above the LCST (~32 °C) (adapted from Ref. [263]).

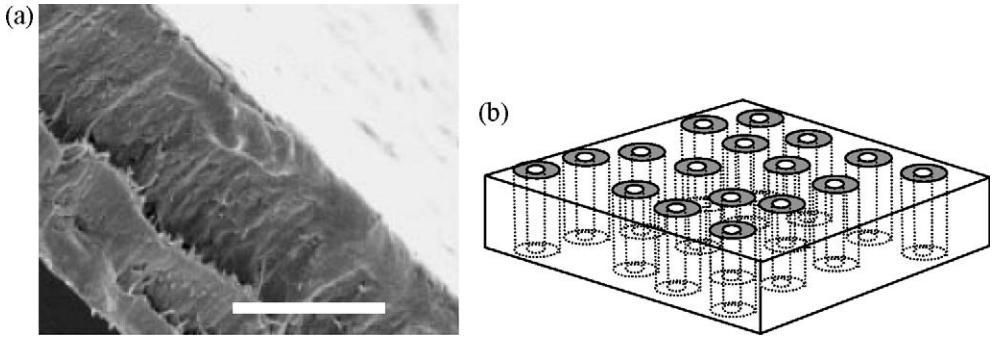

Fig. 34. (a) Cross-sectional SEM image (scale bar: 5 μm) of a ~10 μm thick VA-CNT membrane. Note the CNT alignment across the polystyrene matrix. (b) Schematic representation of a VA-MWNT array being buried in a polystyrene matrix. Hollow cores of VA-MWNTs pass across a continuous polymer film to form a membrane structure (adapted from Ref. [211]).

By infiltration of temperature responsive polymers (*e.g.* poly(N-isopropylacrylamide), PNIPAAm) into VA-CNT arrays, Chen et al. [263] have developed a new class of polymer-CNT smart composities for various multifunctional applications. As schematically shown in Fig. 33A, the VA-CNT array was first set up for the uptake of the potassium persulfate initiator (Fig. 33A(a)), NIPAAm monomer and other reactants to co-initiate the free radical polymerization (Fig. 33A(c)). Thereafter, the infiltrated PNIPAAm chains were confined by an epoxy coating after selective water-plasma-etching of PNIPAAm (Fig. 33A(d and e)). Finally, the epoxy-sealed nanocomposite film was removed from the Si wafer in an aqueous solution of HF and inverted (Fig. 33A(f)) to etch the infiltrated PNIPAAm chains by water-plasma and expose the aligned CNTs (Fig. 33A(g)).

As can be seen in Fig. 33B(a), a uniform nanotube length and surface density for the pristine VA-CNT array were observed. The dry surface of the PNIPAAm/aligned CNT film clearly shows features associated with the water-induced CNT bundles extruding out from the PNIPAAm matrix up to ~300 nm (Fig. 33B(b)). For the wet sample, a much smoother featureless surface, with a reduced roughness of ~10 nm, was shown in Fig. 33B(c). This indicates that the infiltrated PNIPAAm chains had expanded out from the gaps in the VA-CNT forest to cover the nanotube top surface, as schematically shown in Fig. 33B(d–f). This provided the basis for the development of smart nanocomposite films with temperature-induced self-cleaning and/or controlled release capabilities [263].

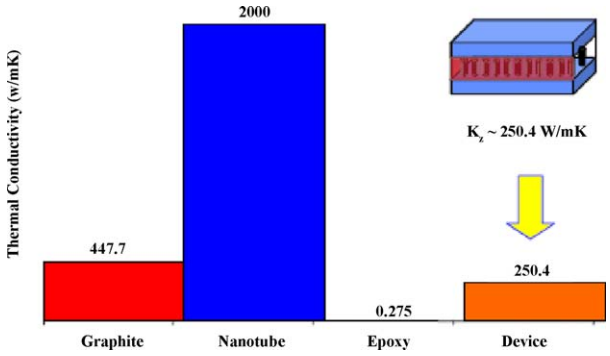

Fig. 35. Comparison of measured through-thickness thermal conductivities of the graphite adherend (facesheet), a MWNT (theoretical), epoxy adhesive, and the expoxy-infiltrated VA-MWNT adhesive joint (adapted from Ref. [277]).

On the other hand, Tu et al. [274] have developed a method to grow low density VA-CNTs, and a polymer-spun-on process to support the aligned structure. If the gaps of the VA-CNTs were filled by polymer, then a well ordered nanoporous membrane was prepared after opening the nanotube tips. By incorporating a high

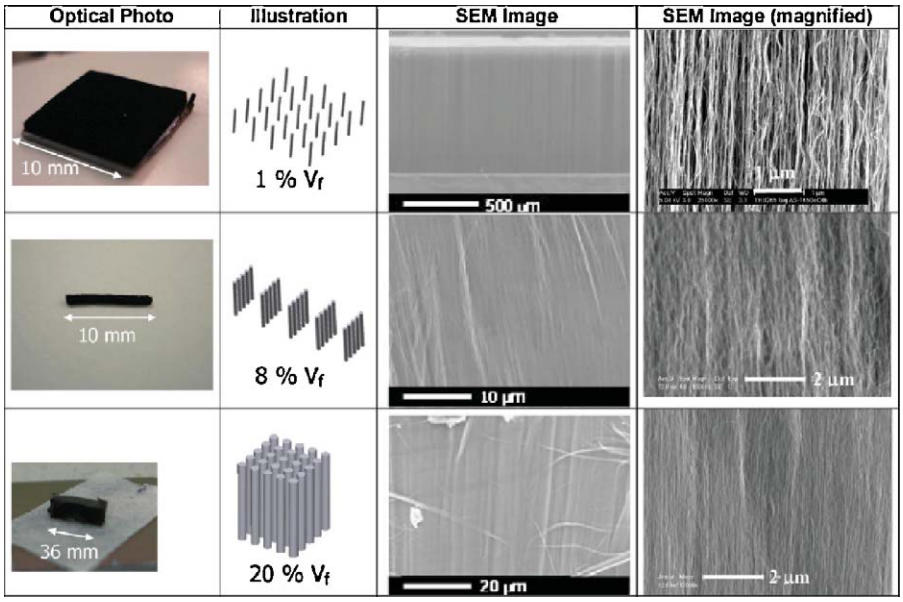

Fig. 36. Aligned CNT volume fraction from mechanical densification of *ca.* 1 mm tall VA-CNT forests at 1% (as-grown), 8% (uniaxially densified), and 20% (biaxially densified) volume fraction (adapted from Ref. [278]).

density array of VA-MWNTs through the thickness of a solid polystyrene film and opening the nanotube end-caps at both sides (*e.g.* by plasma etching), Hinds and co-works [200–202] have indeed successfully prepared VA-MWNT membranes (Fig. 34). Theses authors demonstrated that pressure driven solvent flow can pass through the VA-MWNT membrane 4 to 5 orders of magnitude faster than a simple Newtonian fluid, illustrating the dominance of hydrogen bond ordering. Carbon nanotube based membranes are intriguing since their pore size can be precisely controlled by the controlled nanotube growth and the polarity of the pore can be region-selectively functionalized, as demonstrated by Hinds and others [211,275,276].

Polymer-infiltrated VA-CNTs have also been used to enhance the through-thickness thermal conductivity in the adhesively bonded joints [277]. Fig. 35 shows the measured through-thickness thermal conductivities for a graphite facesheet (447.7 W/m K), an epoxy adhesive (0.275 W/m K), and an expoxy-infiltrated VA-MWNT adhesive joint (250.4 W/m K). Also included in Fig. 35 is a theoretical value of the thermal conductivity for MWNTs (2000 W/m K). As a control, the joint device without using the VA-MWNTs was also measured to yield a thermal conductivity of 0.790 W/m K. Using pyrolitic graphite facesheet, the measured through-thickness thermal conductivity for the joint configuration of VA-MWNTs infused with adhesive was over 250 W/m K. This value of the through-thickness thermal conductivity is a significant improvement compared with the one without the VA-MWNTs, though still lower than that of the graphite facesheet. Both numerical and experimental studies demonstrated that a good thermal contact of the conductive VA-MWNTs with the adherent surfaces is essential to achieve a desirable through-thickness thermal conductivity in joints. Therefore, further work on the tip-functionalization of VA-CNTs should open avenues for the improvement of thermal properties of structural joints and various opportunities for multifunctional applications related to thermal and electrical managements.

For the membrane and thermal joint, and many other applications, high-volume-fraction VA-CNT nanocomposites are highly desirable. An interesting method for mechanical densification of VA-CNT forests has recently been reported by Wardle et al. [278]. The as-grown VA-MWNT volume fraction is typically 1%, giving a coverage of 10^9–10^{10} CNTs/cm^2. To increase the density of a VA-MWNT forest, these authors first released the as-grown VA-MWNT array grown on a Si substrate (1 cm^2) using a standard razor blade from the growth substrate. The released forest was

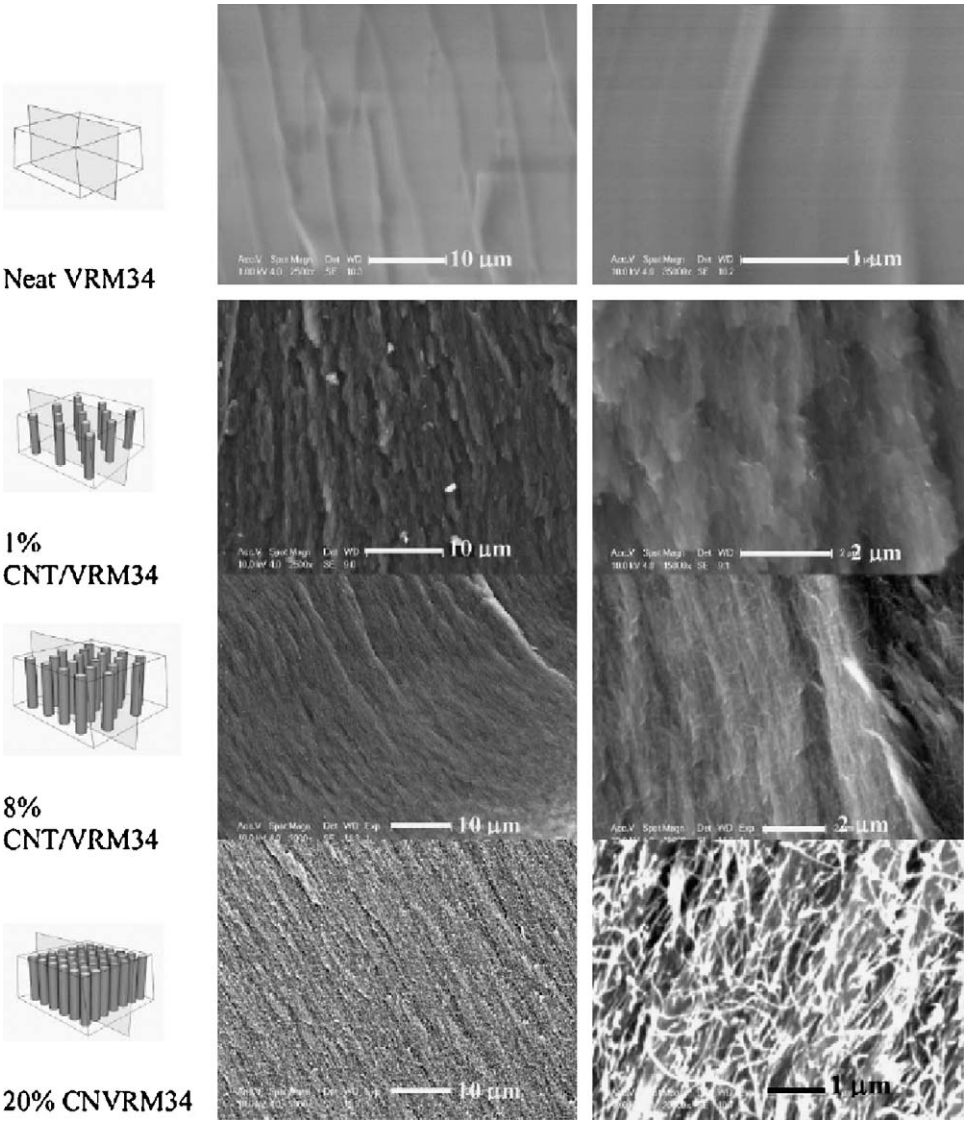

Fig. 37. Fracture surfaces of VA-CNT nanocomposites. Evolution of fracture surface as volume fraction is increased for VRM34 epoxy and VA-CNT nanocomposite (adapted from Ref. [278]).

then placed in a small device that allowed mechanical biaxial compression in two orthogonal directions. By varying the distance the forest is compressed, variable-density CNT forests are obtained, as shown in Fig. 36.

The mechanical densification, in conjunction with appropriate polymer infiltration, allowed VA-CNT nanocomposites of high volume fractions (up to 22%) to be fabricated, as exemplified in Fig. 37. Such VA-CNT nanocomposites should have potential for numerous applications, including thermal and electrical managements.

4. Concluding remarks

We have reviewed recent developments in the controlled growth and functionalization of VA-CNTs for multifunctional applications. As can be seen, a large variety of smart materials and advanced devices could be developed from various multifunctional VA-CNT arrays by controlled nanotube growth, in conjugation with chemical modification of the constituent CNTs. The demonstrated potential applications of VA-CNTs and their derivatives include electron emitting displays, field effect transistors, chemical and biological sensors, membranes for chemical and biological separations, connectors for electrical and thermal managements, new catalysts for fuel cells, smart fibers and films for flexible optoelectronics, and even dry adhesives mimicking gecko foot. With so many methods available for functionalizing and controlling nanotube growth already reported, and more to be developed, there will be vast opportunities for developing numerous new multifunctional materials and devices from VA-CNTs.

Acknowledgements

The authors thank our colleagues, including Wei Chen, Michael Durstock, Pinggang He, Mei Gao, Gordon Wallace, Hans Griesser, Chris Strauss, Shaoming Huang, Xiaoyin Hong, Albert Mau, Qiang Peng, Liangti Qu, Morley Stone, Tia Benson-Tolle, Richard Vaia, Zhenhai Xia, Yadong Yang, Yongyong Yang, and Zhonglin Wang for their contributions to the work cited. We are also grateful for financial support from the NSF (CMS-0609077, CTS0438389, CCF-0403130), MOST of P.R. China (2009DFB30380), R&D Project of Zhejiang Province of P.R. China (2009C13019), AFOSR (FA9550-06-1-0384, FA9550-09-1-0331, FA8650-07-D-5800), AFRL, WCU Project through UNIST from the Ministry of Education, Science and Technology in Korea, and Wenzhou Medical College.

References

[1] P.J.F. Harris, Carbon Nanotubes and Related Structures: New Materials for the Twenty-First Century, Cambridge University Press, New York, 1999.
[2] L. Dai (Ed.), Carbon Nanotechnology: Recent Developments in Chemistry, Physics, Materials Science and Device Applications, Elsevier, Amsterdam, 2006.
[3] S. Iijima, Nature 354 (1991) 56.
[4] R.H. Baughman, A.A. Zakhidov, W.A. de Heer, Science 297 (2002) 787.
[5] L.M. Dai, A. Patil, X.Y. Gong, Z.X. Guo, L.Q. Liu, Y. Liu, D.B. Zhu, Chem. Phys. Chem. 4 (2003) 1150, references cited therein.
[6] Y. Yan, M.B. Chan-Park, Q. Zhang, Small 3 (2007) 24, reference cited therein.
[7] Z.J. Fan, T. Wei, G.H. Luo, F. Wei, J. Mater. Sci. 40 (2005) 5075.
[8] K. Kordas, T. Mustonen, G. Toth, H. Jantunen, M. Lajunen, C. Soldano, S. Talapatra, S. Kar, R. Vajtai, P.M. Ajayan, Small 2 (2006) 1021.
[9] W.R. Small, M.I.H. Panhuis, Small 3 (2007) 1500.
[10] T. Wei, J. Ruan, Z.J. Fan, G.H. Luo, F. Wei, Carbon 45 (2007) 2712.
[11] M. Dragoman, E. Flahaut, D. Dragoman, M. Al Ahmad, R. Plana, Nanotechnology 20 (2009) 37520.
[12] J.N. Coleman, U. Khan, Y.K. Gun'ko, Adv. Mater. 18 (2006) 689.
[13] M. Moniruzzaman, K.I. Winey, Macromolecules 39 (2006) 5194.
[14] M.J. Green, N. Behabtu, M. Pasquali, W.W. Adams, Polymer 50 (2009) 4979.
[15] K.L. Jiang, Q.Q. Li, S.S. Fan, Nature 419 (2002) 801.
[16] M. Zhang, K.R. Atkinson, R.H. Baughman, Science 306 (2004) 1358.
[17] M. Zhang, S.L. Fang, A.A. Zakhidov, S.B. Lee, A.E. Aliev, C.D. Williams, K.R. Atkinson, R.H. Baughman, Science 309 (2005) 1215.
[18] X.B. Zhang, K.L. Jiang, C. Teng, P. Liu, L. Zhang, J. Kong, T.H. Zhang, Q.Q. Li, S.S. Fan, Adv. Mater. 18 (2006) 1505.
[19] Q.W. Li, Y. Li, X.F. Zhang, S.B. Chikkannanavar, Y.H. Zhao, A.M. Dangelewicz, L.X. Zheng, S.K. Doorn, Q.X. Jia, D.E. Peterson, P.N. Arendt, Y.T. Zhu, Adv. Mater. 19 (2007) 3358.
[20] X.F. Zhang, Q.W. Li, T.G. Holesinger, P.N. Arendt, J.Y. Huang, P.D. Kirven, T.G. Clapp, R.F. DePaula, X.Z. Liao, Y.H. Zhao, L.X. Zheng, D.E. Peterson, Y.T. Zhu, Adv. Mater. 19 (2007) 4198.
[21] K. Koziol, J. Vilatela, A. Moisala, M. Motta, P. Cunniff, M. Sennett, A. Windle, Science 318 (2007) 1892.
[22] X.F. Zhang, Q.W. Li, Y. Tu, Y.A. Li, J.Y. Coulter, L.X. Zheng, Y.H. Zhao, Q.X. Jia, D.E. Peterson, Y.T. Zhu, Small 3 (2007) 244.
[23] J.H. Liu, J.Y. Liu, L.B. Yang, X. Chen, M.Y. Zhang, F.L. Meng, T. Luo, M.Q. Li, Sensors 9 (2009) 7343.
[24] K. Balasubramanian, M. Burghard, Anal. Bioanal. Chem. 385 (2006) 452.
[25] S.S. Fan, M.G. Chapline, N.R. Franklin, T.W. Tombler, A.M. Cassell, H.J. Dai, Science 283 (1999) 512.
[26] H. Zhang, G.P. Cao, Y.S. Yang, Energy Environ. Sci. 2 (2009) 932.
[27] L.L. Zhang, X.S. Zhao, Chem. Soc. Rev. 38 (2009) 2520.
[28] J. Liu, G.Z. Cao, Z.G. Yang, D.H. Wang, D. Dubois, X.D. Zhou, G.L. Graff, L.R. Pederson, J.G. Zhang, Chem. Sus. Chem. 1 (2008) 676.
[29] T. Umeyama, H. Imahori, Energy Environ. Sci. 1 (2008) 120.
[30] M. Endo, M.S. Strano, P.M. Ajayan, Top. Appl. Phys. 111 (2008) 13.
[31] F. Cheng, Z. Tao, J. Liang, J. Chen, Chem. Mater. 20 (2008) 667.
[32] H.S. Liu, C.J. Song, L. Zhang, J.J. Zhang, H.J. Wang, D.P. Wilkinson, J. Power Sources 155 (2006) 95.
[33] Q. Cao, J.A. Rogers, Adv. Mater. 21 (2009) 29.
[34] P. Avouris, Z.H. Chen, V. Perebeinos, Nat. Nanotechnol. 2 (2007) 605.
[35] D.C. Wei, Y.Q. Liu, Adv. Mater. 20 (2008) 2815.
[36] D. Tasis, N. Tagmatarchis, V. Georgakilas, M. Prato, Chem. Eur. J. 9 (2003) 4001.
[37] K.F. Fu, Y.P. Sun, J. Nanosci. Nanotechnol. 3 (2003) 351.
[38] T. Lin, V. Bajpai, T. Ji, L. Dai, Aust. J. Chem. 56 (2003) 635.
[39] D. Tasis, N. Tagmatarchis, A. Bianco, M. Prato, Chem. Rev. 106 (2006) 1105.
[40] X.H. Peng, S.S. Wong, Adv. Mater. 21 (2009) 625.
[41] P. Singh, S. Campidelli, S. Giordani, D. Bonifazi, A. Bianco, M. Prato, Chem. Soc. Rev. 38 (2009) 2214.
[42] L.J. Meng, C.L. Fu, Q.H. Lu, Prog. Nat. Sci. 19 (2009) 801.
[43] K. Hata, D.N. Futaba, K. Mizuno, T. Namai, M. Yumura, S. Iijima, Science 306 (2004) 1362.
[44] L. Qu, Q. Peng, L. Dai, G. Spinks, G. Wallace, R.H. Baughman, MRS Bull. 33 (2008) 215, references cited therein.
[45] L. Qu, L. Dai, J. Mater. Chem. 17 (2007) 3401, references cited therein.
[46] K. Gong, S. Chakrabarti, L. Dai, Angew. Chem. Int. Ed. 47 (2008) 5446.
[47] W.A. de Heer, J.-M. Bonard, K. Fauth, A. Châtelain, L. Forró, D. Ugarte, Adv. Mater. 9 (1997) 87, references cited therein.
[48] J. Li, C. Papadopoulos, J.M. Xu, Appl. Phys. Lett. 75 (1999) 367.
[49] T. Iwasaki, T. Motoi, T. Den, Appl. Phys. Lett. 75 (1999) 2044.
[50] T. Kyotani, L.F. Tsai, A. Tomita, Chem. Mater. 8 (1996) 2109.
[51] G. Che, B.B. Lakshmi, E.R. Fisher, C.R. Martin, Nature 393 (1998) 346.
[52] M. Terrones, N. Grobert, J. Olivares, J.P. Zhang, H. Terrones, K. Kordatos, W.K. Hsu, P.P. Hare, P.D. Townsend, K. Prassides, A.K. Cheetham, H.W. Kroto, D.R.M. Walton, Nature 388 (1997) 52.
[53] W.Z. Li, S.S. Xie, L.X. Qian, B.H. Chang, B.S. Zou, W.Y. Zhou, R.A. Zhao, G. Wang, Science 274 (1996) 1701.
[54] T. Kyotani, B.K. Pradhan, A. Tomita, Bull. Chem. Soc. Jap. 72 (1999) 1957.
[55] G. Che, B.B. Lakshmi, C.R. Martin, E.R. Fisher, R.S. Ruoff, Chem. Mater. 10 (1998) 260.
[56] C.N.R. Rao, R. Sen, B.C. Satishkumar, A. Govindaraj, Chem. Commun. 1525 (1998).
[57] R. Kamalakaran, M. Terrones, T. Seeger, Ph. Kohler-Redlich, M. Ruhle, Y.A. Kim, T. Hayashi, M. Endo, Appl. Phys. Lett. 77 (2000) 21.
[58] M. Meyyappan, L. Delzeit, A. Cassell, D. Hash, Plasma Sources Sci. Technol. 12 (2003) 205, references cited therein.
[59] Z.F. Ren, Z.P. Huang, J.H. Xu, P.B. Wang, M.P. Siegal, P.N. Provencio, Science 282 (1998) 1105.
[60] Z.P. Huang, J.W. Xu, Z.F. Ren, J.H. Wang, M.P. Siegal, P.N. Provencio, Appl. Phys. Lett. 73 (1998) 3845.
[61] H. Yasuaki, O. Takayuki, K. Masaaki, H. Hiroyuki, N. Shigehiro, ICPIG Proceedings 25th, Nagoya, Japan, July 17–22 (2001).
[62] Y.H. Wang, J. Lin, C.H.A. Huan, G.S. Chen, Appl. Phys. Lett. 79 (2001) 5.
[63] S.H. Tsai, C.T. Shiu, S.H. Lai, L.H. Chan, W.J. Hsieh, H.C. Shih, J. Mat. Sci. Lett. 21 (2002) 21.
[64] J.Y. Lee, B.S. Lee, Thin Solid Films 418 (2002) 85.
[65] B. Bower, C. Andrew, S. Jin, W. Zhu, PECVD Eur. Pat. Appl. (2001) 18.
[66] Y. Avigal, R. Kalish, App. Phys. Lett. 78 (2001) 2291.
[67] S.M. Huang, L. Dai, A.W.H. Mau, J. Phys. Chem. B 103 (1999) 4223.
[68] Y. Yang, S. Huang, W. He, A.W.H. Mau, L. Dai, J. Am. Chem. Soc. 121 (1999) 10832.
[69] D.C. Li, L. Dai, S.M. Huang, A.W.H. Mau, Z.L. Wang, Chem. Phys. Lett. 316 (2000) 349.
[70] S. Huang, A.W.H. Mau, T.W. Turney, P.A. White, L. Dai, J. Phys. Chem. B 104 (2000) 2193.
[71] Q. Chen, L. Dai, Appl. Phys. Lett. 76 (2000) 2719.
[72] L. Xiao, Z. Chen, C. Feng, L. Liu, Z.Q. Bai, Y. Wang, L. Qian, Y.Y. Zhang, Q.Q. Li, K.L. Jiang, S.S. Fan, Nano Lett. 8 (2008) 4539.
[73] L.M. Ericson, H. Fan, H. Peng, V.A. Davis, W. Zhou, J. Sulpizio, Y. Wang, R. Booker, J. Vavro, C. Guthy, A.N.G. Parra-Vasquez, M.J. Kim, S. Ramesh, R.K. Saini, C. Kittrell, G. Lavin, H. Schmidt, W.W. Adams, W.E. Billups, M. Pasquali, W.F. Hwang, R.H. Hauge, J.E. Fischer, R.E. Smalley, Science 305 (2004) 1447.
[74] Y. Li, I.A. Kinloch, A.H. Windle, Science 304 (2004) 274.

[75] L. Ci, N. Punbusayakul, J. Wei, R. Vajtai, S. Talapatra, P.M. Ajayan, Adv. Mater. 19 (2007) 1719.
[76] L. Qu, L. Dai, M. Stone, Z. Xia, Z.L. Wang, Science 322 (2008) 238.
[77] Y. Zhao, T. Tong, L. Delzeit, A. Kashani, M. Meyyappan, A. Majumdar, J. Vac. Sci. Technol. B 24 (2006) 331.
[78] L. Qu, L. Dai, Adv. Mater. 19 (2007) 3844.
[79] L. Ge, S. Sethi, L. Ci, P.M. Ajayan, A. Dhinojwala, Proc. Natl. Acad. Sci. U.S.A. 104 (2007) 10792.
[80] B. Yurdumakan, N.R. Raravikar, P.M. Ajayan, A. Dhinojwala, Chem. Commun. 30 (2005) 3799.
[81] C. Li, J.M. Papadopoulos, Xu, Nature 402 (1999) 253.
[82] D. Grimm, P. Venezuela, F. Banhart, N. Grobert, H. Terrones, P.M. Ajayan, M. Terrones, A. Latge, Small 3 (2007) 1900.
[83] W.Z. Li, B. Pandey, Y.Q. Liu, J. Phys. Chem. B 110 (2006) 23694.
[84] C. Weisbuch, B. Vinter, Quantum Semiconductor Structures: Fundamentals and Applications, Academic, San Diego, CA, 1991.
[85] J. Hu, M. Ouyang, P. Yang, C.M. Lieber, Nature 399 (1999) 48.
[86] M.H. Huang, S. Mao, H. Feick, H. Yan, Y. Wu, H. Kind, E. Webber, R. Russo, P. Yang, Science 292 (2001) 1897.
[87] M.S. Gudiksen, L.J. Lauhon, J. Wang, D.C. Smith, C.M. Lieber, Nature 415 (2002) 617.
[88] Y. Wu, R. Fan, P. Yang, Nano Lett. 2 (2002) 83.
[89] S. Banerjee, S.S. Wong, Nano Lett. 2 (2002) 195.
[90] A. Jensen, J.R. Hauptmann, J. Nygard, J. Sadowski, P.E. Lindelof, Nano Lett. 4 (2004) 349.
[91] H. Kim, W. Sigmund, Appl. Phys. Lett. 81 (2002) 2085.
[92] J. Du, L. Fu, Z. Liu, B. Han, Z. Li, Y. Liu, Z. Sun, D. Zhu, J. Phys. Chem. B 109 (12) (2005) 772.
[93] A.J. Mieszawska, R. Jalilian, G.U. Sumanasekera, F.P. Zamborini, J. Am. Chem. Soc. 127 (10) (2005) 822.
[94] P.M. Ajayan, O.Z. Zhou, Top. Appl. Phys. 80 (2001) 391.
[95] J. Liu, X. Li, L. Dai, Adv. Mater. 18 (2006) 1740.
[96] Z.Y. Jiang, Z.X. Xie, X.H. Zhang, S.C. Lin, T. Xu, S.Y. Xie, R.B. Huang, L.S. Zheng, Adv. Mater. 16 (2004) 904.
[97] E.T. Thostenson, W.Z. Li, D.Z. Wang, Z.F. Ren, T.-W. Chou, J. Appl. Phys. 91 (2002) 6034.
[98] L. Qu, Y. Zhao, L. Dai, Small 2 (2006) 1052.
[99] G.Y. Zhang, D. Mann, L. Zhang, A. Javey, Y.M. Li, E. Yenilmez, Q. Wang, J.P. McVittie, Y. Nishi, J. Gibbons, H.J. Dai, Proc. Natl. Acad. Sci. 102 (2005) 16141.
[100] P.B. Amama, C.L. Pint, L. McJilton, S.M. Kim, E.A. Stach, P. Murray, R.H. Hauge, B. Maruyama, Nano Lett. 9 (2009) 44.
[101] S. Chakrabarti, H. Kume, L. Pan, T. Nagasaka, Y. Nakayama, J. Phys. Chem. C 111 (2007) 1929.
[102] S. Chakrabarti, T. Nagasaka, Y. Yoshikawa, L. Pan, Y. Nakayama, Jap. J. Appl. Phys. Express Lett. 45 (2007) L720.
[103] S. Chakrabarti, K. Gong, L. Dai, J. Phys. Chem. C 112 (2008) 8136.
[104] Y. Murakami, S. Chiashi, Y. Miyauchi, M.H. Hu, M. Ogura, T. Okubo, S. Maruyama, Chem. Phys. Lett. 385 (2004) 298.
[105] E. Gyula, A.A. Kinkhabwala, H. Cui, D.B. Geohegan, A.A. Puretzky, D.H. Lowndes, J. Phys. Chem. B 109 (2005) 16684.
[106] T. Iwasaki, G.F. Zhong, T. Aikawa, T. Yoshida, H. Kawarada, J. Phys. Chem. B 109 (2005) 19556.
[107] Y.Q. Xu, E. Flor, M.J. Kim, B. Hamadani, H. Schmidt, R.E. Smalley, R.H. Hauge, J. Am. Chem. Soc. 128 (2006) 6560.
[108] M. Cantoro, S. Hofmann, S. Pisana, V. Scardaci, A. Parvez, C. Ducati, A.C. Ferrari, A.M. Blackburn, K.Y. Wang, J. Robertson, Nano Lett. 6 (2006) 1107.
[109] Y. Miyauchi, S. Chiashi, Y. Murakami, Y. Hayashida, S. Maruyama, Chem. Phys. Lett. 387 (2004) 198.
[110] L. Zhang, Y.Q. Tan, D.E. Resasco, Chem. Phys. Lett. 422 (2006) 198.
[111] M. Zheng, A. Jagota, M.S. Strano, A.P. Santos, P. Barone, S.G. Chou, B.A. Diner, M.S. Dresselhaus, R.S. McLean, G.B. Onoa, G.G. Samsonidze, E.D. Semke, M. Usrey, D.J. Walls, Science 302 (2003) 1545.
[112] R. Krupke, F. Hennrich, H. von Lohneysen, M.M. Kappes, Science 301 (2003) 344.
[113] D. Chattopadhyay, L. Galeska, F. Papadimitrakopoulos, J. Am. Chem. Soc. 125 (2003) 3370.
[114] Y. Maeda, S. Kimura, M. Kanda, Y. Hirashima, T. Hasegawa, T. Wakahara, Y.F. Lian, T. Nakahodo, T. Tsuchiya, T. Akasaka, J. Lu, X.W. Zhang, Z.X. Gao, Y.P. Yu, S. Nagase, S. Kazaoui, N. Minami, T. Shimizu, H. Tokumoto, R. Saito, J. Am. Chem. Soc. 127 (2005) 10287.
[115] H.J. Huang, R. Maruyama, K. Noda, H. Kajiura, K. Kadono, J. Phys. Chem. B 110 (2006) 7316.
[116] A.R. Harutyunyan, G.G. Chen, T.M. Paronyan, E.M. Pigos, O.A. Kuznetsov, K. Hewaparakrama, S.M. Kim, D. Zakharov, E.A. Stach, G.U. Sumanasekera, Science 326 (2009) 116.
[117] L. Qu, F. Du, L. Dai, Nano Lett. 8 (2008) 2682.
[118] Y.M. Li, D. Mann, M. Rolandi, W. Kim, A. Ural, S. Hung, A. Javey, J. Cao, D. Wang, E. Yenilmez, Q. Wang, J.F. Gibbons, Y. Nishi, H. Dai, Nano Lett. 4 (2004) 317.
[119] Y. Li, S. Peng, D. Mann, J. Cao, R. Tu, K.J. Cho, H. Dai, J. Phys. Chem. B 109 (2005) 6968.
[120] W.H. Chiang, R.M. Sankaran, Nat. Mater. 8 (2009) 882.
[121] P.H. Tan, A.G. Rozhin, T. Hasan, P. Hu, V. Scardaci, W.I. Milne, A.C. Ferrari, Phys. Rev. Lett. 99 (2007) 137402.
[122] S.M. Bachilo, L. Balzano, J.E. Herrera, F. Pompeo, D.E. Resasco, R.B. Weisman, J. Am. Chem. Soc. 125 (2003) 11186.
[123] X. Li, X. Tu, S. Zaric, K. Welsher, W.S. Seo, W. Zhao, H. Dai, J. Am. Chem. Soc. 129 (2007) 15770.
[124] B. Wang, C.H. Patrick Poa, L. Wei, L.J. Li, Y.H. Yang, Y. Chen, J. Am. Chem. Soc. 129 (2007) 9014.
[125] D. Ciuparu, Y. Chen, S. Lim, G.L. Haller, L. Pfefferle, J. Phys. Chem. B 108 (2004) 503.
[126] R. Seidel, A.P. Graham, E. Unger, G.S. Duesberg, M. Liebau, W. Steinhoegl, F. Kreupl, W. Hoenlein, W. Pompe, Nano Lett. 4 (2004) 831.
[127] S. Kumar, N. Pimparkar, J.Y. Murthy, M.A. Alam, Appl. Phys. Lett. 88 (2006) 123505.
[128] E.S. Snow, J.P. Novak, P.M. Campbell, D. Park, Appl. Phys. Lett. 82 (2003) 2145.
[129] J. Li, Z.B. Zhang, M. Östling, S.L. Zhang, Appl. Phys. Lett. 92 (2008) 133103.
[130] A. Javey, J. Guo, M. Paulsson, Q. Wang, D. Mann, M. Lundstrom, H. Dai, Phys. Rev. Lett. 92 (2004) 106804.
[131] Y. Zhou, A. Gaur, S.-H. Hur, C. Kocabas, M.A. Meitl, M. Shim, J.A. Rogers, Nano Lett. 4 (2004) 2031.
[132] P. He, L. Dai, The Handbook of Biomems and Bio-nanotechnology, in: J. Lee, A. Lee (Eds.), Biomedical and Biological Nanotechnology, Volume 1 of M. Ferrari, Kluwer Academic Publishers, 2005.
[133] J. Kong, H.T. Soh, A.M. Cassell, C.F. Quate, H. Dai, Nature 395 (1998) 878.
[134] X. Xu, G.R. Brandes, Appl. Phys. Lett. 74 (1999) 2549.
[135] M. Burghard, G. Duesberg, G. Philipp, J. Muster, S. Roth, Adv. Mater. 10 (1998) 584.
[136] J. Liu, M.J. Casavant, M. Cox, D.A. Walters, P. Boul, W. Lu, A.J. Rimberg, K.A. Smith, D.T. Colbert, R.E. Smalley, Chem. Phys. Lett. 303 (1999) 125.
[137] J. March, Advanced Organic Chemistry, 4th ed., John Wiley, New York, 1992.
[138] G.M. Wallraff, W.D. Hinsberg, Chem. Rev. 99 (1999) 1801.
[139] Y. Xia, G.M. Whitesides, Annu. Rev. Mater. Sci. 28 (1988) 153.
[140] Y. Xia, G.M. Whitesides, Angew. Chem. Int. Ed. 37 (1998) 550.
[141] R.J. Jackman, G.M. Whitesides, CHEMTECH (May) (1999) 18.
[142] L. Dai, Intelligent Macromolecules for Smart Devices: From Materials Synthesis to Device Applications, Springer-Verlag, New York, 2004.
[143] A. Kumar, G.M. Whitesides, Appl. Phys. Lett. 63 (1993) 2002.
[144] M. Jacoby, C&E News 6 (October) (1997) 34.
[145] A. Kumar, H.A. Biebuyck, G.M. Whitesides, Langmuir 10 (1994) 1498.
[146] E. Kim, Y. Xia, X.-M. Zhao, G.M. Whitesides, Adv. Mater. 9 (1997) 651.
[147] J.A. Rogers, Z. Bao, L. Dhar, Appl. Phys. Lett. 73 (1998) 294.
[148] G. Zheng, H. Zhu, Q. Luo, Y. Zhou, D. Zhao, Chem. Mater. 13 (2001) 2240.
[149] A. Khosla, B.L. Gray, Mater. Lett. 63 (2009) 1203.
[150] A. Mazzoldi, M. Tesconi, A. Tognetti, W. Rocchia, G. Vozzi, G. Pioggia, A. Ahluwalia, D. De Rossi, Mater. Sci. Eng. C 28 (2008) 1057.
[151] H.T. Ng, M.L. Foo, A.P. Fang, J. Li, G.Q. Xu, S. Jaenicke, L. Chan, S.F.Y. Li, Langmuir 18 (2002) 1.
[152] H.T. Ng, A.P. Fang, J. Li, S.F.Y. Li, J. Nanosci. Nanotechnol. 1 (2001) 357.
[153] R.D. Bennett, A.J. Hart, A.C. Miller, P.T. Hammond, D.J. Irvine, R.E. Cohen, Langmuir 22 (2006) 8273.
[154] G.F. Zheng, H.G. Zhu, Q. Luo, Y.M. Zhou, D.Y. Zhao, Chem. Mater. 13 (2001) 2240.
[155] L. Dai, Rad. Phys. Chem. 62 (2001) 55.
[156] J.R. Hollahan, A.T. Bell (Eds.), Techniques and Applications of Plasma Chemistry, John Wiley & Sons, New York, 1974.
[157] F. Ren, Z.P. Huang, D.Z. Wang, J.G. Wen, J.W. Xu, J.H. Wang, L.E. Calvet, J. Chen, J.F. Klemic, M.A. Reed, Appl. Phys. Lett. 75 (1999) 1086.
[158] G. Wen, Z.P. Huang, D.Z. Wang, J.H. Chen, S.X. Yang, Z.F. Ren, J.H. Wang, J.H. Wang, L.E. Calvet, J. Chen, J.F. Klemic, M.A. Reed, J. Mater. Res. 16 (2001) 3246.
[159] B.K. Teo, M. Chhowalla, G.A.I. Amaratunga, W.I. Milne, D.G. Hasko, G. Pirio, P. Legagneux, F. Wyczisk, D. Pribat, Appl. Phys. Lett. 79 (2001) 1534.
[160] S.P. Patole, P.S. Alegaonkar, H.C. Shin, J.B. Yoo, J. Phys. D – Appl. Phys. 41 (2008) 155311.
[161] C.L. Pint, S.T. Pheasant, M. Pasquali, K.E. Coulter, H.K. Schmidt, R.H. Hauge, Nano Lett. 8 (2008) 1879.
[162] S.C. Tseng, C.H. Li, Y.Y. Lin, C.H. Tsai, Z.P. Wang, K.C. Leou, C.H. Tsai, S.P. Chen, J.Y. Lee, B.C. Yao, Diamond Rel. Mater. 14 (2005) 2064.
[163] I. Sohn, C. Choi, S. Lee, T. Seong, Appl. Phys. Lett. 78 (2001) 3130.
[164] Q. Chen, L. Dai, J. Nanosci. Nanotechnol. 1 (2001) 43.
[165] J.M. Havard, S.-Y. Shim, J.M.J. Fréchet, Q. Lin, D.R. Medeiros, C.G. Willson, J.D. Byers, Chem. Mater. 11 (1999) 719.
[166] Z.J. Zhang, B.Q. Wei, G. Ramanath, P.M. Ajayan, Appl. Phys. Lett. 77 (2000) 23.
[167] Q. Wei, R. Vajtai, Y. Jung, J. Ward, R. Zhang, G. Ramanath, P.M. Ajayan, Nature 416 (2002) 495.
[168] J. Yang, L. Dai, R.A. Vaia, J. Phys. Chem. B 107 (2003) 12387.
[169] L. Dai, A.W.H. Mau, Adv. Mater. 13 (2001) 899.
[170] J. Yang, L. Qu, Y. Zhao, Q. Zhang, L. Dai, J.W. Baur, B. Maruyama, R.A. Vaia, E. Shin, P.T. Murray, H. Luo, Z. Guo, J. Nanosci. Nanotechnol. 7 (2007) 1573.
[171] E. Dujardin, T.W. Ebbesen, A. Krishnan, M.M.J. Treacy, Adv. Mater. 10 (1998) 611.
[172] B. Mayers, Y.N. Xia, Adv. Mater. 14 (2002) 279.
[173] W.Q. Han, A. Zettl, Adv. Mater. 14 (2002) 1560.
[174] Z.W. Wang, M.D. Shirley, S.T. Meikle, R.L.D. Whitby, S.V. Mikhalovsky, Carbon 47 (2009) 73.
[175] R.Q. Yu, L.W. Chen, Q.P. Liu, J.Y. Lin, K.L. Tan, S.C. Ng, H.S.O. Chan, G.Q. Xu, T.S.A. Hor, Chem. Mater. 10 (1998) 718.
[176] Y. Wang, J. Wu, F. Wei, Carbon 41 (2003) 2939.
[177] G.H. Xu, Q. Zhang, W.P. Zhou, J.Q. Huang, F. Wei, Appl. Phys. A 92 (2008) 531.
[178] S.C. Tsang, Y.K. Chen, P.J.F. Harris, M.L.H. Green, Nature 372 (1994) 159.
[179] P.X. Hou, C. Liu, H.M. Cheng, Carbon 46 (2008) 2003.
[180] A.F. Ismail, P.S. Goh, J.C. Tee, S.M. Sanip, M. Aziz, Nano 3 (2008) 127.
[181] T. Nakajima, S. Kasamatsu, Y. Matsuo, Eur. J. Solid State Inorg. Chem. 33 (1996) 831.

[182] E.T. Mickelson, C.B. Huffman, A.G. Rinzler, R.E. Smalley, R.H. Hauge, J.L. Margrave, Chem. Phys. Lett. 296 (1998) 188.
[183] E.T. Mickelson, I.W. Chiang, J.L. Zimmerman, P.J. Boul, J. Lozano, J. Liu, R.E. Smalley, R.H. Hauge, J.L. Margrave, J. Phys. Chem. B 103 (1999) 4318.
[184] A. Hirsch, O. Vostrowsky, Top. Curr. Chem. 245 (2005) 193.
[185] S.D. Kim, J.W. Kim, J.S. Im, Y.H. Kim, Y.S. Lee, J. Fluorine Chem. 128 (2007) 60.
[186] W. Zhang, K. Guerin, M. Dubois, Z. El Fawal, D.A. Ivanov, L. Vidal, A. Hamwi, Carbon 46 (2008) 1010.
[187] J. Chen, M.A. Hamon, H. Hu, Y.S. Chen, A.M. Rao, P.C. Eklund, R.C. Haddon, Science 282 (1998) 95.
[188] Y. Chen, R.C. Haddon, S. Fang, A.M. Rao, W.H. Lee, E.C. Dickey, E.A. Grulke, J.C. Pendergrass, A. Chavan, B.E. Haley, R.E. Smalley, J. Mater. Res. 13 (1998) 2423.
[189] Q.D. Chen, L. Dai, M. Gao, S.M. Huang, A. Mau, J. Phys. Chem. B 105 (2001) 618.
[190] P.G. He, L. Dai, Chem. Commun. (2004) 348.
[191] S.M. Huang, L. Dai, A.W.H. Mau, J. Mater. Chem. 9 (1999) 1221.
[192] L. Huang, Dai, J. Nanopart. Res. 4 (2002) 145.
[193] L. Dai, P.G. He, S.N. Li, Nanotechnology 14 (2003) 1081.
[194] M. Gao, L. Dai, G.G. Wallace, Electroanal 15 (2003) 1089.
[195] P. Soundarrajan, A. Patil, L. Dai, J. Vac. Sci. Technol. A 21 (2003) 1198.
[196] S. Li, P. He, J. Dong, Z. Gao, L. Dai, J. Am. Chem. Soc. 127 (2005) 14.
[197] P. He, D.L. Shi, Nanoeng. Struct. Funct. Smart Mater. 45 (2006) 671.
[198] S. Huang, L. Dai, A.W.H. Mau, J. Phys. Chem. B 3543 (2002) 106.
[199] L. Dai, H.J. Griesser, A.W.H. Mau, J. Phys. Chem. 101 (1997) 9548.
[200] B.J. Hinds, N. Chopra, T. Rantell, R. Andrews, V. Gavalas, L.G. Bachas, Science 303 (2004) 62.
[201] M. Majumder, N. Chopra, R. Andrews, B.J. Hinds, Nature 438 (2005) 44.
[202] P. Nednoor, V.G. Gavalas, N. Chopra, B.J. Hinds, L.G. Bachas, J. Mater. Chem. 17 (2007) 1755, references cited therein.
[203] W. Lu, L. Qu, K. Henry, L. Dai, J. Power Source 189 (2009) 1270.
[204] J. Koehne, M. Meyyappan, Nanotechnology 14 (2003) 1239, references cited therein.
[205] I.C. Yeh, G. Hummer, Proc. Natl. Acad. Sci. U.S.A. 17 (2004) 12177.
[206] Y.H. An, S.M. Song, Mol. Cell. Toxicol. 2 (2006) 279.
[207] S. Banerjee, T. Hemraj-Benny, S.S. Wong, Adv. Mater. 17 (2005) 17.
[208] J.L. Bahr, J.M. Tour, J. Mater. Chem. 12 (2002) 1952.
[209] A. Hirsch, Angew. Chem. Int. Ed. 41 (2002) 1853.
[210] K.M. Lee, L.C. Li, L.M. Dai, J. Am. Chem. Soc. 127 (2005) 4122.
[211] N. Chopra, M. Majumder, B.J. Hinds, Adv. Funct. Mater. 15 (2005) 858.
[212] M. Gao, S.M. Huang, L.M. Dai, G. Wallace, R.P. Gao, Z.L. Wang, Angew. Chem. Int. Ed. 39 (2000) 3664.
[213] D. Sazou, C. Georgolios, J. Electroanal. Chem. 429 (1997) 81.
[214] K. Awasthi, T.P. Yadav, P.R. Mishra, S. Awasthi, O.N. Srivastava, Bull. Mater. Sci. 31 (2008) 313.
[215] X.H. Peng, J.Y. Chen, J.A. Misewich, S.S. Wong, Chem. Soc. Rev. 38 (2009) 1076.
[216] G.G. Wildgoose, C.E. Banks, R.G. Compton, Small 2 (2006) 182.
[217] M.J. Moghaddam, S. Taylor, M. Gao, S. Huang, L. Dai, M.J. McCall, Nano Lett. 4 (2004) 89.
[218] J. Li, M. Moskovits, T.L. Haslett, Chem. Mater. 10 (1998) 1963.
[219] H.C. Choi, M. Shim, S. Bangsaruntip, H.J. Dai, J. Am. Chem. Soc. 124 (2002) 9058.
[220] Y.C. Xing, J. Phys. Chem. B 108 (2004) 19255.
[221] R. Azamian, K. Coleman, J. Davis, N. Hanson, M. Green, Chem. Commun. (2002) 366.
[222] B. Kim, W.M. Sigmund, Langmuir 20 (2004) 8239.
[223] L.T. Qu, L.M. Dai, J. Am. Chem. Soc. 127 (2005) 10806.
[224] L.T. Qu, L.M. Dai, E. Osawa, J. Am. Chem. Soc. 128 (2006) 5523.
[225] Y.D. Yang, L.T. Qu, L.M. Dai, T.S. Kang, M. Durstock, Adv. Mater. 19 (2007) 1239.
[226] M.P. Moret, R. Zallen, D.P. Vijay, S.B. Desu, Thin Solid Films 366 (2000) 8.
[227] S.P. Turano, J.D. Flicker, W.J. Ready, Carbon 46 (2008) 723.
[228] W. Feng, X.D. Bai, Y.Q. Lian, J. Liang, X.G. Wang, K. Yoshino, Carbon 41 (2003) 1551.
[229] N.R. Raravikar, L.S. Schadler, A. Vijayaraghavan, Y.P. Zhao, B.Q. Wei, P.M. Ajayan, Chem. Mater. 17 (2005) 974.
[230] H. Yu, W.P. Zhou, G.Q. Ning, Q.F. Zhang, G.H. Luo, F. Wei, Carbon 43 (2005) 2232.
[231] C.V. Nguyen, L. Delzeit, A.M. Cassell, J. Li, J. Han, M. Meyyappan, Nano Lett. 2 (2002) 1079.
[232] C.P. Ewels, M. Glerup, J. Nanosci. Nanotechnol. 5 (2005) 1345.
[233] Y.Y. Shao, J.H. Sui, G.P. Yin, Y.Z. Gao, Appl. Catal. B-Environ. 79 (2008) 89.
[234] S. van Dommele, A. Romero-Izquirdo, R. Brydson, K.P. de Jong, J.H. Bitter, Carbon 46 (2008) 138.
[235] Z.R. Ismagilov, A.E. Shalagina, O.Y. Podyacheva, A.V. Ischenko, L.S. Kibis, A.I. Boronin, Y.A. Chesalov, D.I. Kochubey, A.I. Romanenko, O.B. Anikeeva, T.I. Buryakov, E.N. Tkachev, Carbon 47 (2009) 1922.
[236] A.A. Koos, M. Dowling, K. Jurkschat, A. Crossley, N. Grobert, Carbon 47 (2009) 30.
[237] M. Terrones, A.G. Souza, A.M. Rao, Top. Appl. Phys. 111 (2008) 531.
[238] J. Zhang, X. Liu, R. Blume, A.H. Zhang, R. Schlogl, D.S. Su, Science 322 (2008) 73.
[239] K.P. Gong, F. Du, Z.H. Xia, M. Durstock, L.M. Dai, Science 323 (2009) 760.
[240] L.S. Panchalkarla, A. Govindaraj, C.N.R. Rao, ACS Nano 1 (2007) 494.
[241] S. Basu (Ed.), Recent Trends in Fuel Cell Science and Technology, Springer, New York, 2007.
[242] http://www.americanhistory.si.edu/fuelcells/alk/alk3.htm.
[243] X. Yu, S. Ye, J. Power Sources 172 (2007) 145.
[244] M. Winter, R.J. Brodd, Chem. Rev. 104 (2004) 4245.
[245] J. Zhang, K. Sasaki, E. Sutter, R.R. Adzic, Science 315 (2007) 220.
[246] J. Yang, D.-J. Liu, N.N. Kariuki, L.X. Chen, Chem. Commun. (2008) 329.
[247] A. Kongkanand, S. Kuwabata, G. Girishkumar, P. Kamat, Langmuir 22 (2006) 2392.
[248] J.P. Collman, N.K. Devaraj, R.A. Decreau, Y. Yang, Y.L. Yan, W. Ebina, T.A. Eberspacher, C.E.D. Chidsey, Science 315 (2007) 1565.
[249] B. Winther-Jensen, O. Winther-Jensen, M. Forsyth, D.R. MacFarlane, Science 321 (2008) 671.
[250] J.N. Coleman, U. Khan, Y.K. Gun'ko, Adv. Mater. 18 (2006) 689.
[251] C. Li, E.T. Thostenson, T.W. Chou, Comp. Sci. Technol. 68 (2008) 1227.
[252] T.-W. Chou, L. Gao, E.T. Thostenson, Z. Zhang, J.-H. Byun, Comp. Sci. Technol. 70 (2010) 1.
[253] P.M. Ajayan, L.S. Schadler, C. Giannaris, A. Rubio, Adv. Mater. 12 (2000) 750.
[254] H.D. Wagner, Chem. Phys. Lett. 361 (2002) 57.
[255] C.Y. Li, L.Y. Li, W. Cai, S.L. Kodjie, K.K. Tenneti, Adv. Mater. 17 (2005) 1198.
[256] L. Dai, A.W.H. Mau, J. Phys. Chem. B 104 (2000) 1891.
[257] Y.-P. Sun, K. Fu, Y. Lin, W. Huang, Acc. Chem. Res. 35 (2002) 1096.
[258] S. Niyogi, M.A. Hamon, H. Hu, B. Zhao, P. Bhowmik, R. Sen, M.E. Itkis, R.C. Haddon, Acc. Chem. Res. 35 (2002) 1105.
[259] C. Wei, L. Dai, A. Roy, T.B. Tolle, J. Am. Chem. Soc. 128 (2006) 1412.
[260] L.C. Li, J.B. Yang, R. Vaia, L. Dai, Synth. Met. 154 (2005) 225.
[261] J. Li, H.T. Ng, A. Cassell, W. Fan, H. Chen, Q. Ye, J. Koehne, J. Han, M. Meyyappan, Nano Lett. 3 (2003) 597.
[262] L. Dai, Aust. J. Chem. 60 (2007) 472.
[263] W. Chen, L. Qu, D. Chang, L. Dai, S. Ganguli, A. Roy, Chem. Commun. (2008) 163.
[264] Y.J. Jung, S. Kar, S. Talapatra, C. Soldano, G. Viswanathan, X.S. Li, Z.L. Yao, F.S. Ou, A. Avadhanula, R. Vajtai, S. Curran, O. Nalamasu, P.M. Ajayan, Nano Lett. 6 (2006) 413.
[265] L.T. Qu, L. Dai, Chem. Commun. (2007) 3859.
[266] Q. Peng, L.T. Qu, L. Dai, K. Park, R.A. Vaia, ACS Nano 2 (2008) 1833.
[267] S.G. Chen, J.W. Hu, M.Q. Zhang, M.Z. Rong, Sens. Actuators B 105 (2005) 187, references cited therein.
[268] S. Koul, R. Chandra, S.K. Dhawan, Sens. Actuators B 75 (2001) 151, references cited therein.
[269] J. Kong, N.R. Franklin, C. Zhou, M.G. Chapline, S. Peng, K. Cho, H.J. Dai, Science 287 (2000) 622.
[270] G. Collins, K. Bradley, M. Ishigami, A. Zettl, Science 286 (2000) 1801.
[271] E.S. Snow, F.K. Perkins, S.C. Houser, S.C. Badescu, T.L. Reinecke, Science 307 (2005) 1942.
[272] M. Meyyappan, Carbon Nanotubes: Science and Applications, CRC Press, Boca Raton, FL, 2005.
[273] J. Li, Y. Lu, Q. Ye, L. Delzeit, M. Meyyappan, Electrochem. Solid-State Lett. 8 (2005) H100.
[274] Y. Tu, Y.H. Lin, Z.F. Ren, Nano Lett. 3 (2003) 107.
[275] B. Hinds, in: L. Dai (Ed.), Carbon Nanotechnology: Recent Developments in Chemistry, Physics, Materials Science and Device Applications, Elsevier, Amsterdam, 2006.
[276] S.M. Cooper, B.A. Cruden, M. Meyyappan, R. Raju, S. Roy, Nano Lett. 4 (2004) 377.
[277] S. Sihn, S. Ganguli, A.K. Roy, L. Qu, L. Dai, Comp. Sci. Technol. 68 (2008) 658.
[278] B.L. Wardle, D.S. Saito, E.J. García, A.J. Hart, R.G. de Villoria, E.A. Verploegen, Adv. Mater. 20 (2008) 2707.